[American Journal of Science, Vol. 316, March, 2016, P. 203–240, DOI 10.2475/03.2016.01]

American Journal of Science

MARCH 2016

TWENTY-FIVE MILLION YEARS OF SUBDUCTION-ACCRETION-EXHUMATION DURING THE LATE CRETACEOUS-TERTIARY IN THE NORTHWESTERN CARIBBEAN: THE TRINIDAD DOME, ESCAMBRAY COMPLEX, CENTRAL CUBA

ANA IBIS DESPAIGNE-DÍAZ*,†, ANTONIO GARCÍA-CASCO**,***, DÁMASO CÁCERES GOVEA*, FRED JOURDAN§, SIMON A. WILDE§, and GUILLERMO MILLÁN TRUJILLO§§

ABSTRACT. **The Trinidad dome, Escambray complex, Central Cuba, forms part of an accretionary wedge built-up during intra-oceanic subduction in the Caribbean from the Late Cretaceous (~75 Ma) to Tertiary. Fieldwork, microscopic studies, P-T estimates and new $^{40}Ar/^{39}Ar$ isotopic data indicate a tectono-metamorphic evolution involving five deformation phases. Three main stages (D_1, D_2 and D_3) were responsible for the subduction-exhumation of the units during metamorphic development. $^{40}Ar/^{39}Ar$ isotopic data allow for the first time, an evaluation of the complete time interval from subduction/collision to final exhumation. D_1 deformation took place at 60.5 ± 0.6 Ma during subduction and was characterized by a prograde path with HP peak metamorphic conditions in eclogite facies in the Monforte nappe (the highest structural nappe) and greenschist metamorphism in the La Sierrita, Yaguanabo and Rio Chiquito nappes (at lower structural levels). D_2 deformation (56.32 ± 0.40 Ma) included a short-lived heating event in the lower nappes that caused incipient recrystallization at lower amphibolite facies, but was generally linked to decompression and retrograde metamorphism to greenschist conditions during folding and NNE thrusting of all nappes. Parallelism of the main S_2 foliation and serpentinite lenses indicates D_2 was the main phase of exhumation. During D_3, exhumation and NNE thrusting continued as the units were progressively incorporated into the growing accretionary wedge until about 50 Ma. Structures related to D_4 are post-metamorphic and reflect the domal structure. D_5 strike-slip and normal faults cut the tectonic pile, and low angle normal faults are more abundant towards the dome rim indicating exhumation of the Escambray. Field observations, structures, and the inverted distribution of the P-T conditions in the wedge suggest exhumation mechanisms by underthrusting/underplating and erosion combined with extension at the surface. Subduction/accretion/exhumation in the Trinidad dome thus occurred from 75 to 50 Ma, indicating a period of 25 million years of deformation history in the northern Caribbean realm.**

Keywords: Escambray, accretionary complex, $^{40}Ar/^{39}Ar$ geochronology, Caribbean plate

* Departamento de Geología, Universidad de Pinar del Rio, Cuba, Martí Final # 270, Pinar del Rio, 2100, Cuba
** Departamento de Mineralogía y Petrología, Universidad de Granada, Avda. Fuente nueva sn, 18002 Granada, Spain
*** Instituto Andaluz de Ciencias de la Tierra, CSIC-Universidad de Granada, Granada, Spain
§ Department of Applied Geology, Curtin University, GPO Box U1987 Perth, Western Australia, 6845
§§ Instituto de Geología y Paleontología, Carretera Vía Blanca y Línea de Ferrocarril, Havana, Cuba
† Corresponding author: anaibisd@gmail.com

INTRODUCTION

Accretionary wedges or prisms develop by transfer of materials from the downgoing slab to the upper plate during intraoceanic or continental subduction. Accretion implies downward migration of subduction thrusts resulting in underplating. The rocks accreted to a certain depth may then preserve information on deformation, metamorphism, and exhumation fabrics related to burial, accretion and exhumation. The continuous addition of materials in the accretionary wedge may cause uplift and exhumation with formation of thrust nappes of higher-grade metamorphic units on top of lower-grade units (Kimura and others, 1996; Stanek and others, 2006; Agard and others, 2009). As the early stage of this exhumation process is commonly obscured by important post-collisional events affecting orogenic wedges, extensive petrological, structural and geochronological work is essential to unravel the details of the exhumation processes and their mechanisms.

Oceanic subduction in the Caribbean region during the Cretaceous was interrupted by collision and accretion of Mesozoic sedimentary piles belonging to the passive margin of North America (the sedimentary promontory/terrane named Caribeana, that is Samaná in Hispaniola, Escambray, Asunción, Cangre, and Pinos in Cuba, East Yucatán, and the Puerto Rico trench among others, see García-Casco and others, 2008a and references therein). The process led to the Cretaceous-Tertiary closure of the Proto-Caribbean oceanic basin that occupied the inter-American gap and was connected with the Central Atlantic after the disruption of Pangea, and the related overall collision between the Caribbean plate (Greater Antilles volcanic arc) and the margins of North America (Maya block and Bahamas platform) (for example Iturralde-Vinent and others, 2008). The metamorphic history, age and deformation of the metasedimentary complexes (for example Pyle and others, 1973; Perfit and others, 1980; Joyce, 1991; Cruz-Gamez and others, 2007; García-Casco and others, 2001; Escuder-Viruete and others, 2011a, 2011b) along the leading edge of the Caribbean plate allow the earlier processes of collision/accretion and failure of subduction in the Caribbean during the latest Cretaceous-Tertiary to be deciphered.

In the Trinidad dome of the Escambray complex, Central Cuba, several tectonic units consisting of metasedimentary and metamafic/ultramafic rocks record the insertion of continental margin units into the Caribbean subduction zone (Dublan and others, 1986; Millán, 1997b). The tectonic units are exposed as a nappe stack affected by a late-stage domal structure, and record the whole process of formation and exhumation in an accretionary wedge. In this study we provide new structural and ^{40}Ar-^{39}Ar isotopic data that constrain the metamorphic evolution, deformation and exhumation history of the accretionary complex. Our focus is the less studied lower-grade tectonic unit, and our results complement previous petrological and Ar-Ar cooling ages of higher-grade rocks (eclogites and blueschists) of the structurally higher units of the Escambray complex (Grevel, ms, 2000; Schneider and others, 2004). We, for the first time, evaluate the complete time interval from subduction/collision to final exhumation of the accretionary complex, as well as providing constraints on the timing of collision with the North American plate.

GEOLOGICAL SETTING

Cuba forms part of the Circum-Caribbean orogenic belt that records a long-lasting subduction history at the northern margin of the Caribbean plate (fig. 1A). The origin of the Caribbean plate, however, is a matter of debate (Meschede and Fritz, 1998; Iturralde-Vinent and Lidyak, 2006; Pindell and others, 2005, 2006). The most accepted model emphasizes that the plate formed in the Pacific (Farallon) and that a Cretaceous island arc was originally built due to subduction of the Proto-Caribbean (Atlantic) beneath the Caribbean plate (see review by Boschman and others, 2014 and references therein). Consumption of the Proto-Caribbean allowed the eastward drift of the

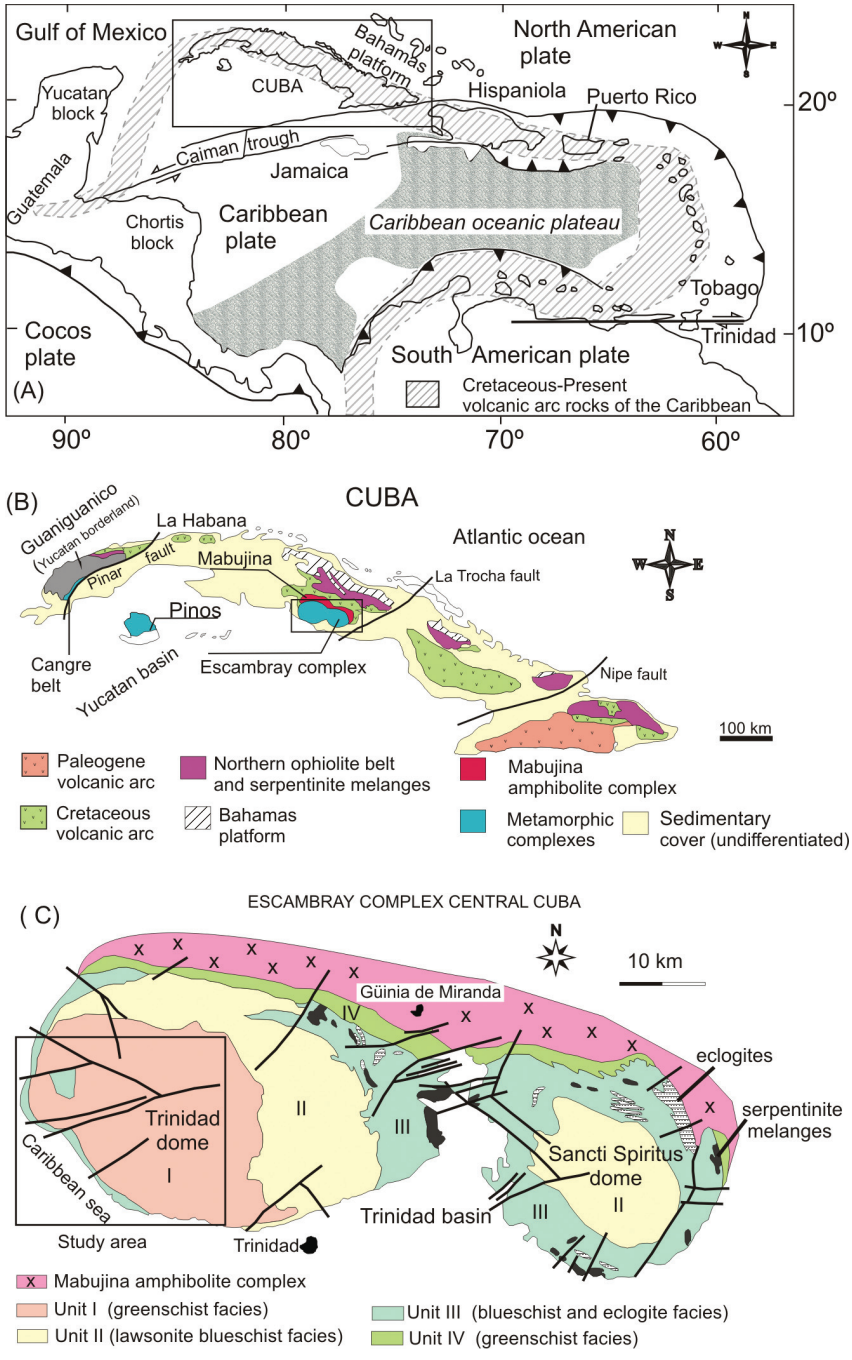

Fig. 1. (A) Plate tectonic configuration of the Caribbean region with important geological features (compiled after Draper and others, 1994; Meschede and Fritz, 1998; Mann, 1999). (B) Geological sketch map of Cuba after Iturralde-Vinent (1996) showing location of the Escambray complex and the Cuban fold and thrust belt. (C) Geological map of the Escambray complex (after Millán, 1997b) with main tectonic units and indication of the study area in the Trinidad dome.

Caribbean plate (relative to the Americas) until the arc finally collided with the passive margin of North America in the Tertiary.

The configuration of the Cuban fold and thrust belt has been studied in detail (Cobiella-Reguera, 1988, 2000, 2005; Iturralde-Vinent, 1994, 1996a; García-Casco and others 2006, 2008; Iturralde-Vinent and others, 2008; Van Hinsbergen and others, 2009). The belt is made up of several elements named from north to south: the Bahamas borderland units, the northern ophiolite complex, the Cretaceous volcanic arc, and the metamorphic complexes to the south and southwest (Iturralde-Vinent, 1994, 1996a, 1988, fig. 1B). In the eastern part of Cuba, the younger (Paleogene) volcanic arc of Sierra Maestra resulted from north-dipping subduction of the Caribbean plate beneath the arc (Cobiella-Reguera, 1988; Sigurdsson and others, 2000; Rojas-Agramonte and others, 2006, 2008). The orogenic belt involves units of continental provenance (Bahamas units and the Caribeanan metamorphic complexes of Pinos, Cangre, Escambray) as well as oceanic units including ophiolites and volcanic arc rocks (Iturralde-Vinent, 1994, 1996a, 1996b). These rocks were amalgamated and appear as complex tectonic slices along the island (fig. 1B). Metamorphic rocks of the Late Cretaceous-Tertiary subduction-collision-accretion event include the sedimentary piles (plus associated passive-margin basic magmas) of the Caribeana terrane and tectonic blocks of oceanic lithosphere within serpentinite melanges (Somin and Millán, 1981; Iturralde-Vinent, 1996a; Millán, 1996a, 1997a, 1997b; García-Casco and others 2002, 2006, 2008a, 2008b). Studies carried out on high pressure (HP) rocks in Cuba and the Dominican Republic serpentinite melanges of the Caribbean subduction channel yield peak and cooling ages ranging from 120 to 80 Ma (García-Casco and others, 2006; Krebs and others, 2008; Lazaro and others, 2009; Blanco-Quintero and others, 2011; Escuder-Viruete and others, 2013). However, peak and cooling ages dating the exhumation of HP rocks in the Caribeanan complexes of Escambray and Pinos (Cuba) and Samaná (Dominican Republic) yield ages younger than 70 Ma (Schneider and others, 2004; Stanek and others, 2006; Stanek and Maresch, 2007; García-Casco and others, 2008a; Escuder-Viruete and others 2011a, 2011b).

The central part of Cuba embraces one of the most complete geological sections in the island where most geological units are present: the para-autochthonous Bahamas platform units to the north, the allochthonous ophiolite complexes (part of the Caribbean plate and Proto Caribbean), the Cretaceous volcanic arc (including the Mabujina arc-derived amphibolite complex) and the Escambray metamorphic complex to the south (fig. 1B). The continental para-autochthonous units comprise Jurassic to Cretaceous folded sedimentary rocks (Bahamas platform) and syn-tectonic Paleocene–Eocene foreland basin sedimentary rocks (Iturralde-Vinent and others, 2008). The overall structure shows increasing deformation from north to south, ranging from a single fold phase to polyphase folding along with thrust faults (Meyerhoof and Hatten, 1968; Iturralde-Vinent and others, 2008; Van Hisbergen and others, 2009). These units are tectonically overlain by allochthonous complexes represented by the ophiolites, highly dismembered sequences that form a melange with remnants of Cretaceous island arc rocks, sediments from the back arc basins (Cruz-Orosa and others, 2012a, 2012b) and serpentinites of the Caribbean fore-arc (García-Casco and others, 2006; Rojas-Agramonte and others, 2010). Within this melange, tectonic slivers of HP rocks occur (García-Casco and others, 2002, 2006).

The ophiolites are overlain by tectonic sheets of Cretaceous volcanic arc rocks composed of Neocomian-Campanian tholeiite and calc-alkaline volcanic rocks and sediments (Fonseca and others, 1989; Kerr and others, 1999). This sequence also tectonically overlies the Mabujina amphibolite complex which is made-up of medium to high grade, low to intermediate pressure metamorphic rocks ranging in composition from ultrabasic to acid and cut by unmetamorphosed and weakly deformed

plutonic bodies (Millán, 1981; Millán, 1996b; Grafe and others, 2001; Blein and others, 2003; Rojas-Agramonte and others, 2011). The complex is considered to represent the metamorphosed base of the Cretaceous volcanic arc (Somin and Millán, 1981; Dublan and others, 1986; Millán, 1996b), but has also been interpreted as a different arc system accreted from the Pacific (Blein and others, 2003; Rojas-Agramonte and others, 2011). The Escambray metamorphic complex crops out in a tectonic window beneath the Mabujina amphibolite complex (figs. 1B and 1C).

The Cuban fold belt was deformed during the latest Cretaceous to middle Eocene when deposition of sedimentary-olistrostomic formations occurred on the ophiolites and autochthonous continental units in the Paleogene (Iturralde-Vinent, 1998a, 1998b).

GEOLOGY OF THE ESCAMBRAY COMPLEX

The Escambray complex covers an area of 1800 km^2. It is the largest metamorphic complex of the Caribbean region. It is composed of strongly deformed continental margin metasediments (metasiliciclastic and metacarbonates) along with metaophiolites and metabasic rocks (Somin and Millán, 1981; Stanik and others, 1981; Millán and Somin, 1985; Dublan and others, 1986; Millán, 1996b, 1997b; Schneider and others, 2004; García-Casco and others, 2006; Stanek and others, 2006). It is divided into two structural domes, the Trinidad dome to the west and the smaller and less-eroded Sancti Spiritus dome to the east. They are flanked by the Tertiary Trinidad sedimentary basin (fig. 1C). Based on fossils found in the metacarbonates, the protolith ages of these rocks are Jurassic to Early Cretaceous. Stratigraphic arguments allow correlation of the sequence with those of western Cuba belonging to the Guaniguanico complex, which formed part of the passive margin of the Maya block during the Jurassic-Cretaceous (Millán and Myczinsky, 1978; Stanik and others 1981; Millán and Somin, 1985; Somin and others, 1992; Pszczolkowski, 1999).

The main aspects of the internal structure, nappe arrangement and petrography of the Escambray complex were established by Somin and Millán (1972, 1981), Stanik, (1981), Millán and Somin (1985), and Dublan and others (1986). Millán and Somin (1985) divided the complex into several tectonic units and metamorphic zones. Millán (1997b) proposed a new tectonic subdivision that comprises four tectonic units (or mega-units, fig. 1C) each composed of several tectonic slices. Each mega-unit consists of different lithostratigraphic formations that show an inverted metamorphic pattern. Unit I, the lower structural unit, is composed of greenschist-facies rocks of pelitic and carbonate composition (fig. 1C). Unit II includes metasedimentary rocks with boudins of basic and ultrabasic rocks metamorphosed in the lawsonite-blueschist facies. Unit III forms an irregular rim surrounding both the Trinidad and Sancti Spiritus domes and is composed of the same rock-types as Unit II, but includes eclogitic bodies either preserved in a serpentinite matrix, or interlayered with the metasedimentary sequence. HP conditions reported from the eclogites indicate temperatures of 530 to 630° and pressures of 15 to 23 kbar (Grevel, ms, 2000; Schneider and others, 2004; García-Casco and others, 2006; Stanek and others, 2006). Unit IV diverges from the general pattern and forms a thin greenschist-facies strip to the north, in tectonic contact with the Mabujina amphibolite complex (fig. 1C). Stanek and others (2006) suggested a different tectonic arrangement for the Sancti Spiritus dome, formed by the lowermost Pitajones nappe (similar to Unit II of Millán, 1997b), Gavilanes nappe (eclogite facies similar to Unit III of Millán, 1997b) and the uppermost Yayabo unit (garnet-amphibolites) belonging to the Escambray complex [previously defined by Millán and Somin (1985)]. They considered that tectonic transport to the N-NE is supported by kinematic indicators.

HP conditions reported in eclogites indicate subduction of the passive continental margin sequence as well as oceanic lithosphere, as indicated by serpentinites and

enclosed HP metamorphic tectonic blocks (Schneider and others, 2004; García-Casco and others, 2006). Despite the Late Jurassic ages (U-Pb zircon 140–160 Ma) for eclogite, Maresh and others, 2003) and Mid-Late Cretaceous ages (U-Pb zircon 106–100 Ma, Hatten and others, 1988, 1989), most age data reported from the Escambray cluster around 85 to 65 Ma (K-Ar 85–68 Ma, $^{40}Ar/^{39}$ Ar 71–68 Ma; Rb/Sr 65–69 Ma; Lu-Hf *ca.* 70 Ma; Somin and Millán, 1981; Hatten and others, 1988, Somin and others, 1992; Iturralde-Vinent and others, 1996; Schneider and others, 2004; Stanek and others, 2007), indicating subduction and exhumation during the Late Cretaceous-Tertiary. The U-Pb zircon Jurassic and Mid-Cretaceous ages most likely represent the crystallization of the magmatic protoliths of the subducted rocks (Millán, 1996a, 1996b; Schneider and others, 2004; García-Casco and others, 2006). The geochronological data from eclogites demonstrate cooling and exhumation at 70 Ma when subduction was still active (Schneider and others, 2004; García-Casco and others, 2006, 2008a; Stanek and others, 2007).

The Trinidad dome incorporates the four (I-IV) main tectonic units of the Escambray complex. The dome has been extensively eroded and uplifted compared to the neighboring Sancti Spiritus dome, and erosional levels have exposed the lowermost structural greenschist Unit I (fig. 1C). In the study area, tectonic Unit I outcrops extensively along with a strip of Unit III bordering the dome and forming a tectonic klippen with an area of about 6 to 7 km^2 in the center of the study area (fig. 1C). Rock-types comprise metacarbonates, metabasites, calcschists, quartz-mica schists, marbles and metacherts in Unit I, and quartz mica schists, marbles, graphitic schists, metabasites, and minor eclogite bodies in Unit III. Millán and Alvarez-Sánchez (1992) discussed the major aspects of the stratigraphy and general structure of the area. These authors identified (from bottom to top in the tectonic pile) the Rio Chiquito, Yaguanabo, and La Sierrita nappes (belonging to the greenschist-facies Unit I) and the uppermost Monforte nappe (belonging to eclogite-bearing tectonic Unit III, fig. 2). Major contact zones are marked by strongly sheared serpentinite horizons and/or lenses, intense folding and numerous kinematic indicators such as σ-type porphyroclasts and duplex structures. Within the nappes, sheared serpentinite lenses define minor tectonic slices (fig. 2).

FIELD RELATIONS

The lowermost ***Rio Chiquito nappe*** exposes a series of pelitic schists, marbles, carbonate mica schists, metasilicates and basic metavolcanic rocks. Strongly sheared serpentinite lenses are ubiquitous. The structurally intermediate ***Yaguanabo nappe*** is mainly composed of basic metavolcanic greenschist facies rocks (fig. 2) together with marbles, and calcschists that make up 40 percent of the nappe. Talc- and actinolite-bearing rocks and epidotites occur along tectonic contacts. Overlaying the Yaguanabo nappe, the ***La Sierrita nappe*** is composed of calcschists, metasandstones, pelitic schists and marbles, together with interleaved metabasic rocks up to several meters thick derived from basalts and/or tuffs that indicate volcanic activity associated with the continental margin (Stanik and others, 1981; Millán and Somin, 1985; Millán, 1997b). Mylonitic serpentinites are also common along major tectonic contacts. At the top of the nappe pile, the ***Monforte nappe*** consists of HP metasediments and largely retrogressed eclogites and metabasites (fig. 2). Mica schists are the major rock type together with graphitic, quartz-muscovite schists, marbles, and calcareous schists. The eclogitic rocks occur within the metasediments as thin layers and/or boudins that can reach meters in size. In the eastern segment a series of metasandstones and marbles crop out in tectonic contact below the Rio Chiquito nappe, and have been grouped as an undifferentiated nappe. The main lithologies consist of thick layers of marble (fig. 2) and also metasandstones. The structure of all nappes shows a top to the NNE tectonic

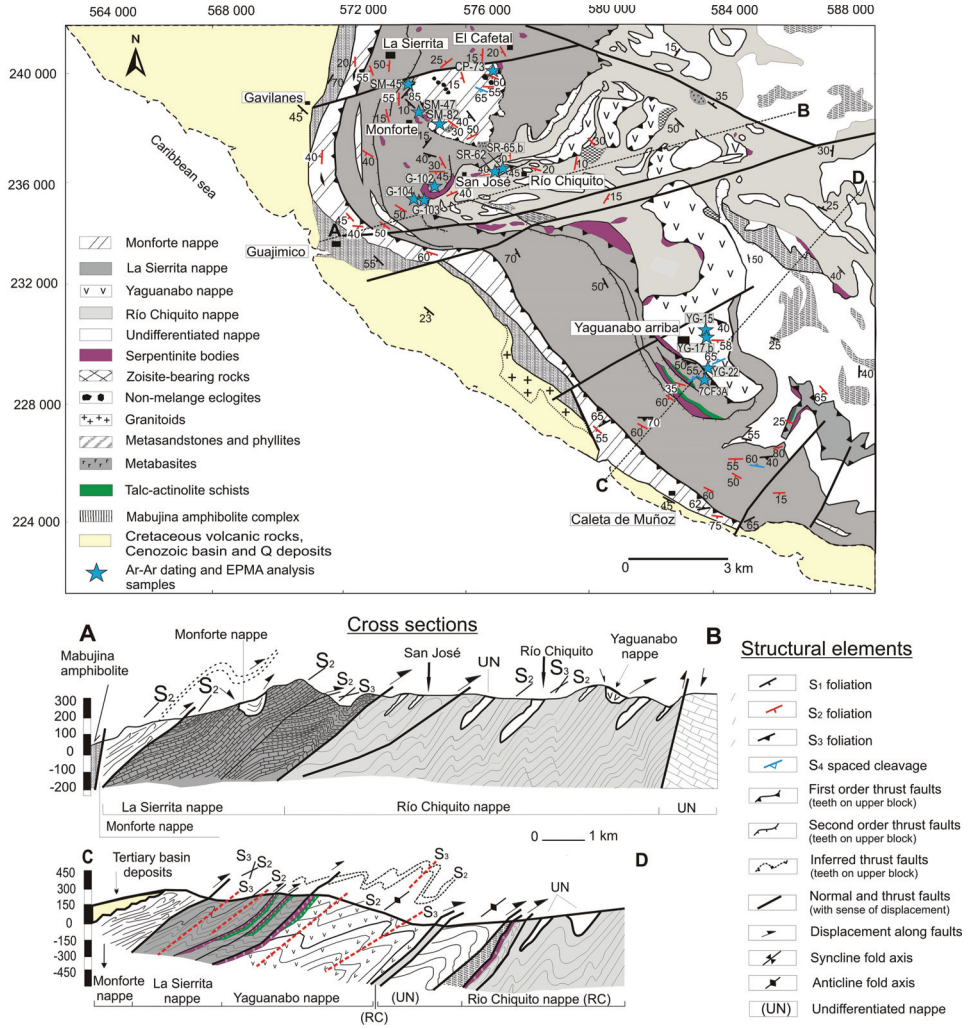

Fig. 2. Simplified geological and tectonic map of the southwest Trinidad dome (modified from Millán and Alvarez-Sanchez, 1992) with units described in the text together with two typical cross sections. The principal foliations S_1, S_2 and S_3, and the location of samples for $^{40}Ar/^{39}Ar$ dating and EMPA analysis are also indicated.

transport (fig. 2). Post-metamorphic strike-slip and normal faults cross-cut the whole sequence (Despaigne-Diaz, ms, 2009).

DEFORMATION HISTORY

Deformation Phases

Our field and microscopic observations allow us to constrain the structural evolution of the Trinidad dome into five deformation phases: D_1-D_5. Overprinting criteria at macro- meso- and micro-scale have been used to unravel the overall structure. D_1-D_3 deformations are syn-metamorphic and show alignment/recrystallization of metamorphic minerals along foliation planes. D_4-D_5 are post-metamorphic and reflect periods of brittle-ductile and brittle deformation, respectively.

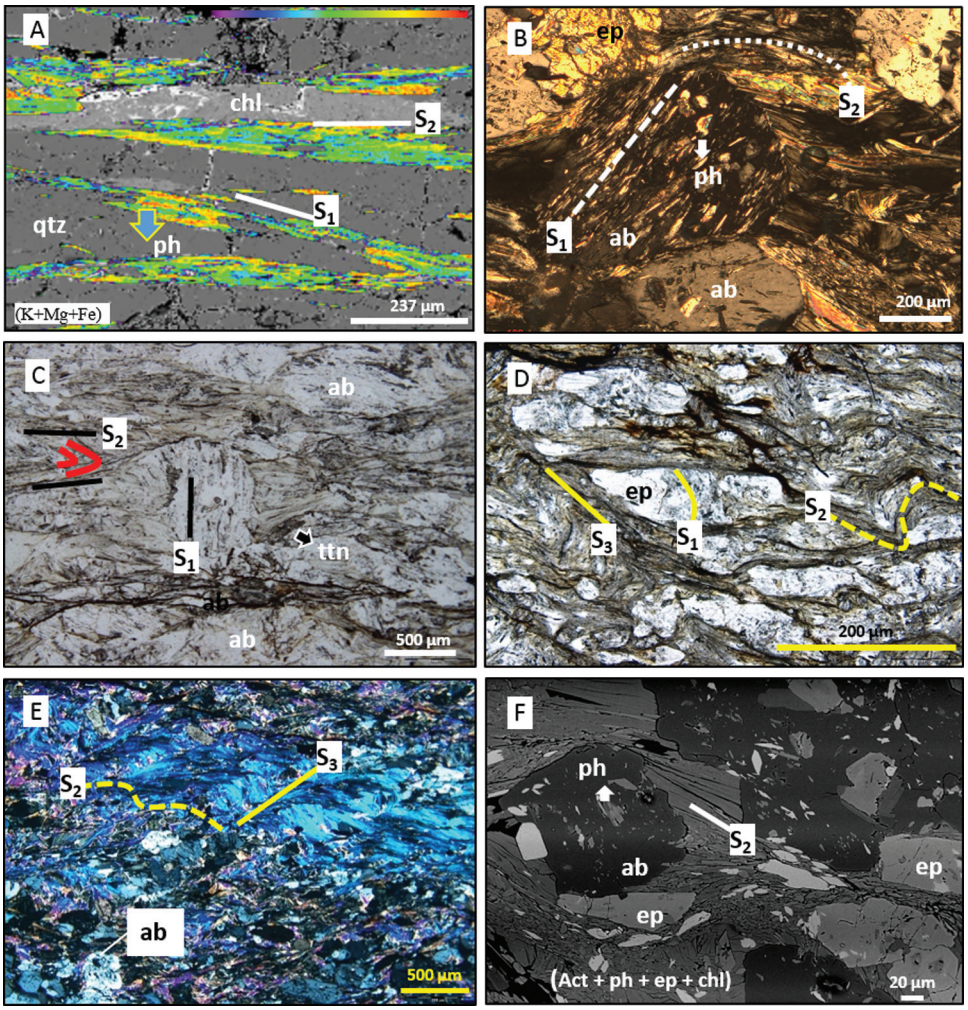

Fig. 3. Microphotographs of representative foliations in the metasediments from the Trinidad dome. (A) Composite X-ray image of S_1 foliation at a low angle to S_2 in quartz mica-schist, the La Sierrita nappe. Color scale represents counts/nA per s and indicates high (red) and low (purple) concentrations. (B) Relic S_1 foliation inside albite porphyroblast in metabasite from the Yaguanabo nappe. (C) Micaschist from the La Sierrita nappe with S_1 foliation inside albite and a completely new foliation, S_2, in the matrix. Note the folded phengites inside microlithons and the S_2 foliation running horizontal to the photo view. (D) Three ductile foliations in metabasite from the Rio Chiquito nappe. S_1 is defined by actinolite inside epidote porphyroblasts. S_2 is intensively folded and a new S_3 surface develops, (E) S2 and S3 foliations in metapelite from the Rio Chiquito nappe. (F) S_2 main foliation in calcschist from the La Sierrita nappe. Mineral abbreviations after Whitney and Evans (2010).

D_1 deformation.—The earliest D_1 structures are represented by a relic S_1 foliation, intrafolial and rootless isoclinal folds and boudins. The primary sedimentary surface (S_0) is commonly parallel to S_1 and is best observed in metasandstones, calcschists and metacarbonates that show S_1 veins of quartz and calcite parallel to S_0. The S_2 foliation wraps around boudins retaining the S_1 foliation. Detailed inspection at outcrop scale shows relics of S_1 foliation transposed into the main S_2 foliation. At the microscopic scale the S_1 foliation is observed at a low angle to the S_2 foliation (fig. 3A) or within the S_2 microlithons in micaschist and calcschists in all nappes (fig. 3C). It is also common

inside albite and epidote porphyroblasts in mica schists and metabasites (figs. 3B and 3D). The S_1 mineral assemblage is defined by phengite, actinolite, Fe-oxides (hematite) and Fe-sulphides (figs. 3B, 3D, and 3F). S_1 phengites inside albite porphyroblasts display a folded pattern, though S_1 trails may also be straight (figs. 3B, 3D, and 3F) and completely discordant relative to S_2 in the matrix, suggesting different stages of porphyroblast growth during deformation. The HP metabasites of the Monforte nappe preserve S_1 glaucophane inside garnet now mostly transformed to a greenschist assemblage of actinolite-epidote-phengite-albite-chlorite (fig. 4F). D_2 structures have obscured/destroyed the previous D_1 structures and transposed the S_1 foliation. The D_1 folds are poorly preserved thus no sense of shear can be deduced.

D_2 deformation.—D_2 is the main deformation phase in all units, and is related to exhumation. A penetrative S_2 foliation is the main tectonic feature in the field. In the upper Monforte nappe, S_2 is more intensely folded, but it has a generally consistent dip to the southwest in the La Sierrita, Yaguanabo and the Rio Chiquito nappes. The S_2 foliation is developed in the hinge zone of large-scale F_2 folds and is parallel to D_2 thrust faults, where strongly sheared serpentinite and actinolite-bearing schist bodies are parallel to S_2. Kinematic indicators in these mylonitic rocks indicate top to the north and northeast tectonic transport (fig. 2). Deformation increases toward the higher structural levels of the nappe pile. A NW-SE trending mineral lineation defined by actinolite occurs in the metabasites and calcschists of the greenschist-facies nappes.

In the greenschist-facies nappes, S_2 is best defined by phengite, along with actinolite, calcite, chlorite, epidote, garnet, quartz and titanite in calcschists, and by phengite, actinolite, chlorite, albite, biotite, titanite and magnesio-hornblende in metabasites (figs. 3E and 3F). A common feature in calcschists, mica schist and metabasites is the presence of large albite porphyroblasts aligned in the S_2 foliation. They contain relics of the S_1 foliation (randomly oriented or folded) defined by phengite, epidote, and graphite, discordant to the S_2 foliation. They may also contain syn-D_2 folded inclusions of phengite, actinolite and epidote concordant with the S_2 foliation in the matrix. These different cases indicate a complex history of albite growth and deformation and that they may have grown either as intertectonic crystals (post D_1-Pre D_2) or syntectonic with D_2 deformation according to the schemes of Zwart (1960, 1962) and Passchier and Trouw (1998) (figs. 3B, 3C, 3D, 3F, and 4B).

D_3 deformation.—D_3 deformation is also intense in all units, and a ductile axial planar S_3 foliation developed in the hinges of D_3 folds (figs. 3D and 3E). Folds are tight to overturned to the NE with fold axes dipping gently to the northwest or southeast. An L_3 intersection lineation defines the intersection between S_2 and S_3 planes. They show similar orientation to the D_3 fold axes. At the mesoscopic scale, the asymmetry of regionally overturned D_3 folds indicates tectonic movement to the north and northeast (fig. 2). This is also supported by the orientation of shear joints and conjugate shear sets in the greenschist-facies units with a general top to the north-northeast sense of shear. Low angle thrust faults are also abundant (Despaigne-Díaz and Caceres Govea, 2009a).

At the microscopic scale the phengites define an S_3 surface (figs. 3D and 3E). They are bent in the fold hinges with or without recrystallization. Mineral growth is observed in the pressure shadows of porphyroblasts and greenschist-facies overprint (Fe-rich chlorite) surrounds or replaces garnet porphyroblasts. The D_3 structures and mineral assemblages in the Monforte nappe indicate this deformation took place during retrogression of the HP assemblages to greenschist facies.

D_4 deformation.—D_4 is associated with a S_4 regionally spaced cleavage that affects the previously folded and metamorphosed sequences. It is best observed in marbles, and is consistent with a transition from a brittle-ductile to a brittle environment at shallow structural levels, with formation of open folds with vertical axial planes. In the fold hinges calcite en-echelon veins are observed. Extensional joints are also abundant.

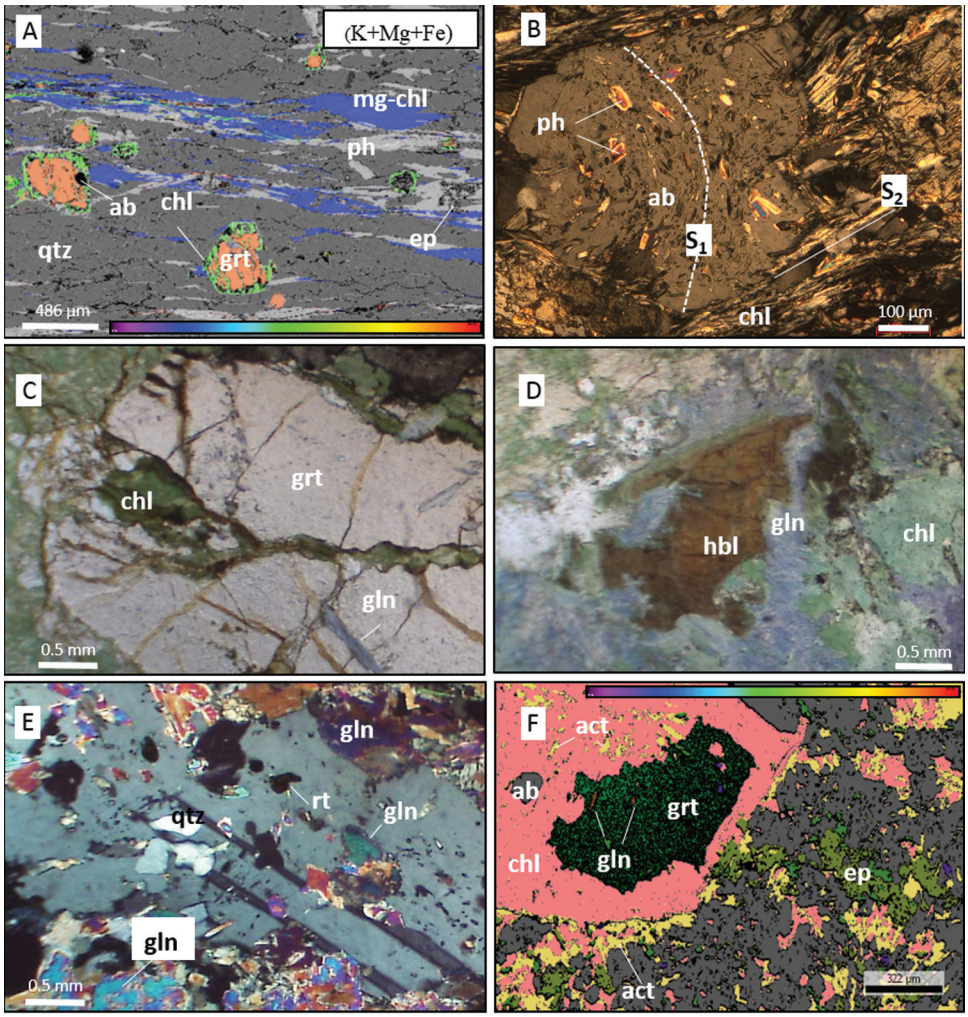

Fig. 4. Metamorphic textures in metasediments from the Trinidad dome. (A) Composite X-ray image of K+Mg+Fe showing retrograde garnet porphyroblasts in quartz mica-schist, the La Sierrita nappe. Color scale represents counts/nA per s and indicates high (red) and low (purple) concentrations. S_2 foliation defined by quartz (dark gray), Mg-rich chlorite (green), epidote (medium gray), garnet (orange) and phengite (light gray). Retrograde Fe-rich chlorite (green) and albite (black). (B) S_1 foliation inside albite porphyroblast discordant with the external S_2 foliation in metabasite of the Yaguanabo nappe. (C) Retrograde chlorite and glaucophane in garnet cracks in eclogite from the Monforte nappe. (D) Magmatic hornblende replaced by glaucophane and chlorite in glaucophane schist from the Monforte nappe. (E) Plagioclase porphyroblast with rutile, quartz and glaucophane inclusions in eclogite from the Monforte nappe. (F) X-ray image showing idiomorphic garnet almost totally replaced by chlorite. Relic S_1 glaucophane inside garnet in retrograde metabasite from the Monforte nappe. Mineral abbreviations after Whitney and Evans (2010).

The regional distribution of the S_4 cleavage reflects the formation of the Trinidad dome during exhumation and is probably related to extension at shallow levels. At the microscopic scale, extension veins filled with quartz and calcite cross-cut previous structures (Despaigne-Diaz and Caceres Govea, 2009b).

D_5 deformation.—D_5 is the latest deformation recognized in the field and is characterized by left- and right-lateral strike-slip faults with northwest-southeast sense

of movement according to associated synthetic Riedel shears related to the major strike-slip faults in the area, measured slickensides on the fault planes, and low angle normal faults affecting all nappes. Locally, folds with steep fold axes ($\geq 70°$) developed, associated with the strike-slip faults (Despaigne-Díaz and Caceres Govea, 2009a). Low-angle normal faults with dip angles $\leq 25°$ are common. It is unclear whether these faults are related to the strike-slip stage (where transpression and transtension occur along the fault plane and normal faults developed) or correspond to a later stage of relaxation where only normal faults occur, hence a discrimination of an additional deformation phase is not supported by geological evidence or the overprinting relationships.

METAMORPHIC EVOLUTION

Eighty samples were collected throughout the study area in order to characterize regional metamorphism of the HP Monforte nappe and the greenschist-facies units.

HP Metamorphism of the Monforte Nappe

High-pressure metamorphism in the Monforte nappe is established by the occurrence of retrogressed eclogites and metabasites. These rocks are either weakly or strongly foliated and reworked to lower grade mafic schists. Peak metamorphism is indicated by the presence of relic garnet and rutile (fig. 4E) (though relic omphacite is cited by Millan (1997b). Glaucophane inclusions within garnet attest for prograde metamorphism through the blueschist facies (figs. 4E and 4F). The eclogite facies assemblage was overprinted by post-peak actinolite, glaucophane, chlorite, epidote, albite, phengite, quartz, titanite, and minor pyrite, indicating retrogression to blueschist and greenschist facies conditions. Relic hornblende (from the protolith or an early intermediate/low-P event) is locally present partly transformed into glaucophane and chlorite (fig. 4D). This is in agreement with similar features of eclogites from the Sancti Spiritus dome (Schneider and others, 2004). Retrogression through the blueschist and greenschist facies took place during D_2 and D_3 deformation.

Greenschist Facies Nappes

Prograde greenschist-facies metamorphism characterizes the three lower units (the La Sierrita, Yaguanabo and Rio Chiquito nappes) in the southwestern Trinidad dome. The mineral paragenesis is actinolite, phengite, chlorite, epidote, albite, and titanite. Depending on bulk composition, garnet, quartz and calcite may also be present. The metamorphic evolution during greenschist facies can be constrained according to the three main D_1-D_3 deformation phases. D_1 mineral assemblages in the S_1 foliation are defined mostly by phengite and actinolite, present as straight, or folded inclusions inside albite and epidote porphyroblasts (figs. 3C, 3D, and 4B), or inside microlithons (fig. 3C), or the S_1 phengites may be randomly oriented (fig. 3F), indicating prograde metamorphism. The presence of magnesio-hornblende and biotite aligned along the S_2 foliation in metabasites suggests a transition to amphibolite facies and a temperature increase during D_2. D_3 mineral assemblages are mostly reoriented minerals along the S_3 planes or newly recrystallized phengites in the D_3 fold hinges.

MINERAL CHEMISTRY

Twelve samples from all nappes were selected for mineral analyses (fig. 2). Description of procedures is included in Appendix 1A. Representative analyses are given in tables 1–6. Atoms per formula unit is abbreviated apfu in the text below.

Mineral Compositions

Garnet.—Garnets were analyzed from metabasites and calcschists of the Monforte nappe and from mica schists from the La Sierrita nappe. Mineral composition is

TABLE 1

Representative analyses of garnet

	SM-82				CP-73			SM-45		
Rock type	metabasite				calcschist			grt mica schist		
Nappe	M				M			LS		
Texture	core	core	core	rim	rim	core	rim	core	core	rim
Phase	garnet									
SiO_2	37.80	37.10	37.69	37.61	37.16	37.59	38.08	35.83	36.39	36.90
TiO_2	0.13	0.18	0.12	0.17	0.15	0.22	0.08	0.53	0.33	0.13
Al_2O_3	20.97	20.63	21.18	20.94	20.86	20.97	21.29	20.16	20.29	20.67
FeO	28.07	28.41	27.98	28.20	29.04	27.69	27.40	16.21	15.82	23.45
MnO	0.76	1.55	0.59	0.96	1.18	1.14	0.68	23.60	19.74	11.80
MgO	1.91	1.61	2.06	1.86	2.95	2.67	2.85	0.28	0.30	0.48
CaO	11.46	10.72	11.14	11.17	8.16	9.72	9.79	3.37	7.35	7.50
Total	101.16	100.23	100.79	100.93	99.54	100.08	100.27	100.06	100.25	100.97
Si	2.97	2.95	2.97	2.96	2.96	2.97	3.00	2.93	2.94	2.96
Ti	0.01	0.01	0.01	0.01	0.01	0.01	0.00	0.03	0.02	0.01
Al	1.94	1.93	1.96	1.94	1.96	1.96	1.98	1.95	1.94	1.95
Fe^{3+}	0.12	0.15	0.09	0.12	0.11	0.08	0.03	0.13	0.14	0.12
Fe^{2+}	1.73	1.74	1.75	1.74	1.83	1.75	1.78	0.98	0.93	1.46
Mn	0.05	0.10	0.04	0.06	0.08	0.08	0.05	1.64	1.35	0.80
Mg	0.22	0.19	0.24	0.22	0.35	0.31	0.33	0.03	0.04	0.06
Ca	0.96	0.91	0.94	0.94	0.70	0.82	0.83	0.30	0.64	0.64
Mg #	0.11	0.10	0.12	0.11	0.16	0.15	0.16	0.03	0.04	0.04
Xalm	0.58	0.59	0.6	0.58	0.62	0.59	0.6	0.33	0.32	0.49
Xsp	0.02	0.04	0.03	0.02	0.03	0.03	0.02	0.56	0.46	0.27
Xgr	0.33	0.31	0.32	0.32	0.41	0.24	0.28	0.10	0.22	0.22

Abbreviations for all tables as follow:
M: Monforte, LS: La Sierrita, YG: Yaguanabo, RC: Rio Chiquito, S_2: matrix S_2, S_3: matrix S_3, incl. Ab: inside albite, grt: garnet

normalized to 8 cations and 12 oxygens, and Fe^{3+} calculated by stoichiometry. Garnet in metabasites and calcschists is relatively rich in almandine (Xsp=0.24–0.33) and grossular (Xgrs=0.10–0.25) and poor in sperssartine (Xsp=0.02–0.04), and has Mg # (Mg/(Mg+Fe) ranging from 0.10–0.13 (fig. 5A, table 1). In contrast, garnet from the mica schists is rich in spessartine (Xsp=0.27–0.56) and almandine (Xalm=0.32–0.49), with minor grossular (Xgrs=0.10–0.22, fig. 5A, table 1) and has a lower Mg # (≤0.05, table 1). In all lithologies grossular and Fe^{2+} contents tend to increase toward the grain rims (table 1), although zoning is faint. The presence of mica-filled strain shadows around garnets suggest growth and deformation during, or shortly/after, peak metamorphism.

Phengite.—Phengite composition is plotted in figures 5C and 5D as a function of rock-type and position in the foliation. The structural formula of phengite is normalized to 22 oxygens and $Fe_{total}=Fe^{2+}$. It is rich in celadonite content, with Si≥6.50 (up to 7.3 in sample Sr-65), Mg = 0.50–0.93, Fe^{2+} = 0.18–0.47 apfu, and is poor in paragonite (Na = 0.01–0.10), indicating high-pressure conditions (Guiddottti, 1978, figs. 5C, 5D, and table 2). Phengites show variable chemical composition according to their microstructural position (fig. 5D). D_1 crystals inside albite have Si contents ranging from 6.56 up to 6.88 apfu (maximum in sample YG-17b, table 2). Phengites in the S_2 planes have Si = 6.55–7.3 apfu though most values range from 6.60 to 6.87 apfu. S_3 phengites have Si contents over a more restricted interval ranging from 6.52 to 6.80 apfu (fig. 5D, table 2). These chemical data suggest reorientation of older mica grains

TABLE 2

Representative analyses of phengite

Sample	SM-45		YG-17b	G-102	SR-65			SM-82		CP-73		YG-15		YG-22
Rock Type	grt m-schist		calschist	calschist	metapelites			metabasite		calschist		metabasite		
Nappe	LS		YG	LS	RC			M		M		YG		
Texture	S_2	S_2	incl Ab	S_2	S_2	S_2	S_2	inside	grt	S_2	S_2	incl Ab		incl Ab
Phase							phengite							
SiO_2	50.17	47.98	51.02	48.62	49.74	46.81	47.75	48.41	49.38	49.40	53.78	46.21	47.96	46.68
TiO_2	0.08	0.12	0.05	0.00	0.17	0.12	0.15	0.10	0.13	0.47	0.15	0.00	0.00	0.23
Al_2O_3	28.53	30.14	26.07	26.97	26.55	28.02	28.02	29.68	30.08	28.76	22.03	29.57	32.37	3.18
FeO_{total}	2.17	1.54	3.00	4.16	2.33	3.68	2.68	2.34	2.24	1.85	2.93	2.14	1.09	2.47
MnO	0.06	0.08	0.04	0.00	0.03	0.04	0.03	0.03	0.01	0.00	0.01	0.00	0.00	0.00
MgO	2.70	2.44	3.37	4.45	3.17	3.32	2.85	2.47	2.42	2.49	4.61	3.19	2.36	1.66
CaO	0.01	0.01	0.02	0.00	0.10	0.04	0.01	0.04	0.06	0.03	0.01	0.50	0.00	0.08
BaO	0.70	0.70	0.13	0.00	0.29	0.28	0.28	0.22	0.21	0.40	0.22	0.00	0.00	0.04
Na_2O	0.30	0.32	0.15	0.34	0.23	0.29	0.22	0.38	0.38	0.51	0.04	0.46	0.64	0.75
K_2O	9.41	9.49	11.14	9.75	10.26	9.91	10.28	10.64	10.22	10.54	10.41	9.81	0.62	10.31
H_2O*	4.45	4.39	4.55	4.40	4.37	4.31	4.32	4.43	4.49	4.44	4.44	4.33	4.48	4.43
Total	98.60	97.22	99.52	98.68	97.23	96.71	96.58	98.74	99.61	98.89	98.64	96.40	99.23	98.84
Si	6.76	6.55	6.88	6.62	6.82	6.52	6.62	6.56	6.60	6.67	7.3	6.40	6.41	6.32
Ti	0.01	0.01	0.01	0.00	0.02	0.01	0.02	0.01	0.01	0.05	0.02	0.00	0.00	0.02
Al	4.53	4.85	4.14	4.33	4.29	4.60	4.58	4.74	4.74	4.57	3.51	4.86	5.07	5.13
Fe^{2+}	0.24	0.18	0.34	0.47	0.27	0.43	0.31	0.27	0.25	0.21	0.33	0.25	0.12	0.28
Mn	0.01	0.01	0.00	0.00	0.00	0.00	0.00	0.00	0.00	0.00	0.001	0.00	0.00	0.00
Mg	0.54	0.50	0.68	0.90	0.65	0.69	0.59	0.50	0.48	0.50	0.93	0.66	0.47	0.34
Ca	0.00	0.00	0.01	0.00	0.01	0.00	0.00	0.01	0.01	0.00	0.002	0.07	0.00	0.01
Ba	0.04	0.04	0.01	0.00	0.02	0.01	0.02	0.01	0.01	0.02	0.012	0.00	0.00	0.002
Na	0.08	0.09	0.04	0.09	0.06	0.05	0.06	0.10	0.10	0.13	0.01	0.12	0.14	0.198
K	1.62	1.92	1.80	1.69	1.80	1.76	1.82	1.84	1.74	1.81	1.79	1.73	1.81	1.78
Mg#	0.69	0.67	0.64	0.68	0.71	0.62	0.66	0.65	0.66	0.71	0.74	0.73	0.79	0.55

* Calculated by stoichiometry. S_3: matrix S_3. Other abbreviations as in table 1.

TABLE 3

Representative analyses of amphibole

Sample	SM-82			G-102	YG-22	YG-15		SR-62		SM-82	
Rock Type	metabasite			calc-shist	meta-basite	metabasite		metabasite		metabasite	
Nappe	M			LS	YG	YG		RC		M	
Texture	inside garnet			incl Ab	S_2	incl Ab	incl Ab	S_2	incl Ab	incl Ab	grt rim
Phase	glaucophane			actinolite		actinolite		Magnesio-Hb		actinolite	
SiO_2	57.76	57.98	57.68	54.47	54.94	54.97	55.26	52.09	49.23	55.99	55.81
TiO_2	0.05	0.05	0.03	0.00	0.02	0.00	0.00	0.05	0.10	0.02	0.00
Al_2O_3	9.73	10.41	9.58	2.86	0.89	0.97	2.85	4.78	5.95	1.49	1.44
FeO_{total}	12.36	12.12	12.23	10.74	9.13	9.30	9.64	11.71	13.82	10.37	11.39
MnO	0.08	0.08	0.03	0.26	0.21	0.29	0.28	0.25	0.25	0.12	0.08
MgO	10.61	10.03	10.70	16.39	18.17	18.44	17.49	16.04	13.66	17.63	16.95
CaO	2.46	1.44	2.55	11.70	12.72	12.53	11.81	10.30	10.90	11.59	11.39
BaO	0.00	0.00	0.00	0.00	0.00	0.00	0.00	0.00	0.00	0.00	0.01
Na_2O	5.64	6.25	5.67	0.90	0.22	0.52	1.25	0.49	1.48	0.67	0.82
K_2O	0.06	0.05	0.04	0.00	0.05	0.00	0.00	0.18	0.42	0.07	0.08
H_2O*	2.18	2.18	2.18	2.10	2.09	2.10	2.14	2.05	2.03	2.13	2.12
Total	100.94	100.58	100.6	99.43	98.43	99.12	100.72	96.97	97.84	100.07	100.09
Si	7.95	7.97	7.95	7.76	7.87	7.84	7.74	7.49	7.28	7.90	7.90
Ti	0.01	0.01	0.00	0.00	0.00	0.00	0.00	0.01	0.01	0.00	0.00
Al	1.58	1.69	1.56	0.48	0.15	0.16	0.47	0.83	1.04	0.25	0.24
Fe^{3+}	0.01	0.01	0.03	0.11	0.09	0.03	0.10	0.17	0.27	0.08	0.10
Fe^{2+}	1.41	1.39	1.38	1.17	1.01	1.08	1.03	1.26	1.44	1.15	1.25
Mn	0.01	0.01	0.00	0.03	0.03	0.03	0.03	0.03	0.03	0.01	0.01
Mg	2.18	2.06	2.20	3.48	3.88	3.92	3.65	3.51	3.01	3.71	3.58
Ca	0.36	0.21	0.38	1.79	1.95	1.92	1.77	1.63	1.73	1.75	1.73
Ba	0.00	0.00	0.00	0.00	0.00	0.00	0.00	0.00	0.00	0.00	0.00
Na	1.50	1.67	1.51	0.25	0.06	0.14	0.34	0.14	0.43	0.18	0.23
K	0.01	0.01	0.01	0.00	0.01	0.00	0.00	0.03	0.08	0.01	0.02
Mg #	0.61	0.60	0.61	0.75	0.79	0.78	0.78	0.74	0.74	0.74	0.68
Na(A)	0.00	0.00	0.01	0.04	0.07	0.03	0.13	0.14	0.06	0.23	0.03
Na(B)	1.50	1.66	1.51	0.05	0.19	0.03	0.01	0.20	0.08	0.20	0.22

* Calculated by stoichiometry. Abbreviations as in table 1.

and (re)crystallization during S_1-S_3 development (figs. 3D and 3E). The high Si content in D_1 phengites indicates high pressure at this early stage, while the lower minimum values of Si in S_2 and S_3 phengites suggests (re)crystallization and associated structural development during exhumation (figs. 5C and 5D).

Amphibole.—Amphibole composition varies from actinolite, magnesio-hornblende to glaucophane following the classification of Leake and others (1997). In samples from the greenschist-facies nappes, it is calcic in composition (actinolite), with a few analyses clasified as magnesio-hornblende in metabasites of the Rio Chiquito nappe, whereas it is glaucophane in metabasites of the Monforte nappe (fig. 5B). The structural formula is normalized to 23 oxygens. Actinolite has Mg = 3.65–3.92, Na (A) = 0.03–0.23 apfu and Na (B) = 0.04–0.22 apfu (table 3). Magnesio-hornblende has Si = 7.28–7.48 apfu, Al total between 0.82–1.20 apfu, Ti contents as low as 0.01 apfu, and Mg # = 0.66–0.74 (table 3, sample SR-62). Zoning is not common, though locally some crystals show weak zoning with actinolite cores and magnesio-hornblende rims indicative of prograde conditions during D_2. This fact, together with the orienta-

TABLE 4

Representative analyses of plagioclase

Sample	SR-65			G-102		CP-73	
Rock Type	metapelite			calcshist		calcshist	
Nappe	RC			LS		M	
Texture	rim	rim	core	S_2	S_2	S_2	S_2
Phase				albite			
SiO_2	68.89	68.22	68.44	67.56	66.10	67.86	68.71
Al_2O_3	19.52	19.35	19.25	20.40	19.54	19.14	19.48
FeO_{total}	0.05	0.10	0.12	0.00	0.39	0.09	0.42
MnO	0.01	0.00	0.01	0.00	0.00	0.00	0.00
CaO	0.11	0.06	0.14	0.00	0.22	0.08	0.08
BaO	0.00	0.01	0.00	0.00	0.00	0.00	0.00
Na_2O	11.88	11.94	11.65	12.03	11.31	12.00	11.75
K_2O	0.06	0.08	0.11	0.00	0.00	0.08	0.07
Total	100.52	99.77	99.73	99.99	97.57	99.27	100.53
Si	2.99	2.99	3.00	2.96	2.96	2.99	2.99
Al	1.00	1.00	0.99	1.05	1.03	0.99	1.00
Fe^{3+}	0.00	0.00	0.00	0.00	0.01	0.00	0.02
Mn	0.00	0.00	0.00	0.00	0.00	0.00	0.00
Ca	0.01	0.00	0.01	0.00	0.01	0.00	0.00
Ba	0.00	0.00	0.00	0.00	0.00	0.00	0.00
Na	1.00	1.02	0.99	1.02	0.98	1.03	0.99
K	0.00	0.00	0.01	0.00	0.00	0.00	0.00

Abbreviations as in table 1.

tion of crystals along the S_2 foliation is a major argument for a slight temperature increase (accompanied by decompression, as indicated by phengite) during D_2 deformation. D_1 actinolite inside albite porphyroblasts shows slight variations in composition but comparable with D_2 crystals (table 3).

Pre-peak (prograde) inclusions of glaucophane within garnet from metabasites of the Monforte nappe (fig. 5B) have Na (B) = 1.50–1.76; Al = 1.56–1.69, Ca = 1.50–1.67–0.38 apfu and Mg # = 0.60–0.61 (table 3).

Plagioclase.—Plagioclase was normalized to 5 cations and 8 oxygens and $Fe_{total}=Fe^{2+}$. Peak plagioclase from the greenschist-facies units and retrograde plagioclase from the Monforte nappe show no zoning and are pure albite in composition with Xab $\geq$ 0.98 (table 4).

Chlorite.—Chlorite occurs along S_2 and S_3 planes of all units, and is stable in transitional assemblages containing magnesio-hornblende. Mineral compositions are normalized to 20 oxygens and 16 OH. Si content varies from 5.43–5.67, Al = 4.57–5.24, Mn = 0.00–0.18, and Mg # = 0.53–0.71 (table 5). Retrograde chlorite replacing garnet in the Monforte unit (sample SM-82) shows the lowest Mg # value (0.53 apfu, table 5). Fe is $\geq$ 2 apfu in all samples and can reach up to 4.47 apfu (table 5). Mn shows variations ranging from 0.04 to 0.08 apfu in metapelites, metabasites and calcschists and 0.18 apfu in quartz-mica schists. These variations correlate with bulk composition (Fe-richer compositions are present in Fe-rich samples containing garnet). Chlorite along the S_2 foliation has Mg # = 0.62–0.69 in metabasites and calcschists. Chlorite along the S_3 foliation in metapelites has values ranging from 0.57 to 0.59 apfu (table 5).

Epidote.—Epidote was normalized to 12.5 oxygens and $Fe_{total}=Fe^{3+}$. Epidote inclusions (50 μm in size) within albite porphyroblasts show high Al contents (2.50–

TABLE 5

Representative analyses of chlorite

Sample	SR-62	YG-15	YG-22	SM-82		SR-65			SM-45		G-103
Rock Type		metabasites		metabasite		metapelite (grt)			mica schist		calcschist
Nappe	RC	YG	YG	M	M	RC			LS		LS
Texture	S_2	S_2	S_2	rg	grt rim	S_3	S_3	S_3	S_2	S_2	incl Ab
Phase	chlorite										
SiO_2	27.15	28.70	28.94	26.89	26.53	26.61	26.76	26.51	27.90	26.96	27.25
Al_2O_3	19.67	21.70	18.78	19.25	19.56	20.97	20.37	19.14	21.11	21.62	20.97
FeO_{total}	19.62	18.21	16.39	24.89	25.32	21.70	21.70	22.69	18.41	19.30	1.56
MnO	0.22	0.00	0.22	0.41	0.44	0.23	0.21	0.23	1.02	1.01	0.25
MgO	18.46	21.18	20.16	15.67	15.70	17.79	17.43	16.62	18.31	17.93	22.10
H_2O*	11.43	11.87	11.62	11.38	11.37	11.59	11.48	11.25	11.74	11.65	12.04
Total	96.79	102.01	96.71	98.93	99.04	99.04	98.20	97.10	98.91	98.65	100.66
Si	5.70	5.64	5.98	5.67	5.60	5.51	5.59	5.65	5.70	5.55	5.43
Al	4.87	5.02	4.57	4.78	4.86	5.12	5.01	4.81	5.08	5.24	4.93
Fe^{2+}	3.44	2.99	2.83	4.39	4.47	3.76	3.79	4.05	3.15	3.32	2.67
Mn	0.04	0.00	0.04	0.07	0.08	0.04	0.04	0.04	0.18	0.18	0.04
Mg	5.78	6.20	6.21	4.93	4.94	5.49	5.43	5.28	5.58	5.50	6.57
Mg #	0.63	0.67	0.69	0.53	0.53	0.59	0.59	0.57	0.64	0.62	0.71

* Calculated by stoichiometry. rg: replacing garnet. Other abbreviations as in table 1.

TABLE 6

Representative analyses of biotite and epidote

Sample	YG-17b		SR-62	YG-22		G-102		SR-65			SM-82
Rock Type	calcschist			metabasites		calcschist		metapelite			metabasite
Nappe	YG		RC	YG		LS		RC			M
Texture	S_2	S_2	S_2	S_2	S_2	rim	S_2	S_2	incl Ab	inside grt	
Phase			biotite			epidote					
						G-II	G-I	G-II	G-1	G-II	G-I
SiO_2	37.18	35.90	29.59	38.34	38.23	36.77	38.51	38.12	38.65	37.78	38.51
TiO_2	1.25	1.10	0.02	1.00	0.95	0.00	0.03	0.12	0.00	0.05	0.27
Al_2O_3	15.25	14.98	18.63	14.79	14.91	24.89	28.42	24.15	31.04	24.79	31.51
FeO_{total}	16.85	17.87	18.41	12.65	12.65	10.12	5.60	11.27	3.68	9.56	2.15
MnO	0.12	0.13	0.25	0.13	0.10	0.00	0.06	0.14	0.00	0.09	0.00
MgO	10.78	11.89	17.45	14.68	14.84	0.00	0.03	0.03	0.00	0.05	0.00
CaO	23.99	23.96	23.95	23.87	23.53	23.99	23.65	23.27	24.61	23.38	25.60
BaO						0.00	0.02	0.00	0.00	0.00	0.00
Na_2O	0.11	0.12	0.09	0.15	0.09						
K_2O	7.35	0.90	0.84	7.93	8.14						
H_2O*	3.72	3.40	0.84	3.89	3.89	1.87	1.92	1.90	1.93	1.88	1.96
Total	92.49	82.55	89.21	94.01	94.18	97.64	98.32	99.07	99.19	97.63	100.00
Si	5.79	5.02	4.83	5.92	5.89	2.95	3.01	3.01	3.01	3.01	2.95
Ti	0.13	0.00	0.00	0.12	0.11	0.00	0.00	0.01	0.01	0.00	0.02
Al	2.85	3.85	3.59	2.69	2.71	2.35	2.62	2.25	2.53	2.33	2.84
Fe^{2+}	2.41	2.54	2.52	1.63	1.63						
Fe^{3+}						0.68	0.37	0.74	0.44	0.64	0.14
Mn	0.02	0.03	0.03	0.02	0.01	0.00	0.00	0.01	0.00	0.01	0.00
Mg	2.59	3.13	4.25	3.38	3.41	0.00	0.00	0.00	0.00	0.01	0.00
Ca						2.06	1.98	1.97	1.99	2.00	2.10
Ba						0.00	0.001	0.00	0.00	0.00	0.00
Na	0.03	0.04	0.03	0.04	0.03						
K	1.51	0.20	0.18	1.56	1.60						
Mg #	0.52	0.55	0.63	0.67	0.68						

* Calculated by stoichiometry. Abbreviations as in table 1.

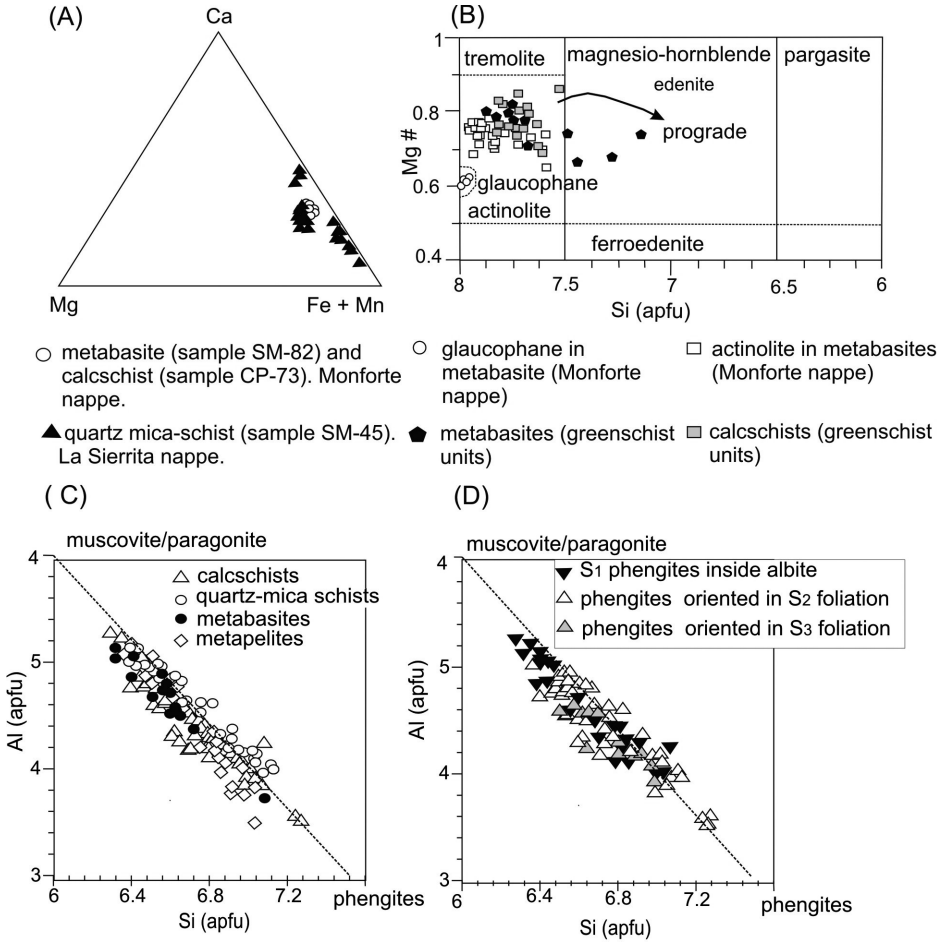

Fig. 5. (A) Composition of garnet from metabasites and calcschists from the Monforte nappe (samples SM-82 and CP-73) and quartz mica-schist from the La Sierrita nappe (sample SM-45) in terms of spessartine + almandine (Mn + Fe), grossular (Ca) and pyrope (Mg) contents. (B) Composition of amphiboles from metabasites and calcschists from the Monforte nappe and the greenschist units. Note the prograde path from actinolite to magnesio-hornblende in metabasites (see text for discussion). (C) Compositional variation of phengite in all units and all rock types. (D) Compositional variation in phengite according to different foliations in all rock types. Note the high Si values between 6.4 and 7.3 apfu.

2.83) and low Fe^{3+} (0.14–0.37, table 6) and are classified as clinozoisite, whereas matrix S_2 and S_3 epidotes (250–300 μm in size) are richer in Fe and are classified as epidote *senso stricto*, with Fe^{3+} = 0.64–0.74 and Al = 2.25–2.35 (table 6). Retrograde epidote in the Monforte nappe metabasites (in garnet pseudomorphs, sample SM-82), shows variable Fe^{3+} (0.14–0.64) and Al (2.33–2.84, table 6) contents.

Biotite.—Biotite is rare and only found in metabasites bearing magnesio-hornblende of the Rio Chiquito nappe (sample SR-62, table 6). Mineral composition is normalized to 20 oxygens and 4 OH and Fe_{total}=Fe^{2+}. Al in biotite ranges from 2.71 to 3.85 apfu and Mg # = 0.52–0.68 (table 6). Ti ranges from 0.00 to 0.13 apfu (table 6) indicating low temperature (Guidotti and others, 1977). Mass deficiency detected in some analyses (total sum of oxides = 82–92%, table 6) may indicate vacancies in the 12-coordinated site of the mineral structure (Guidotti and Dryar, 1991; Dryar and

others, 1991), the presence of Fe^{3+} in rocks containing magnetite/hematite (Guidotti, 1984), and/or chloritization at the submicroscopic scale. The fact that biotite is intergrown with chlorite, and often appears at chlorite rims indicates prograde replacement and that the mass deficiency is largely controlled by chlorite intergrowths at the submicroscopic scale.

$^{40}Ar/^{39}Ar$ GEOCRONOLOGY

Samples and Results

The aim of our study was to date the D_1, D_2 and D_3 deformation events. Phengite is the only mineral that is found in all metamorphic foliations (S_1, S_2 and S_3) and is amenable to $^{40}Ar/^{39}Ar$ dating. Eight samples from the La Sierrita, and the Rio Chiquito nappes were selected to perform $^{40}Ar/^{39}Ar$ geochronology (figs. 2 and 6). They all underwent polyphase deformation and greenschist-facies metamorphism. All samples show a strong S_2 planar fabric and are fine-grained. They were crushed and sieved at different fractions (125, 212 and 350 μm, although 212 μm was most commonly chosen). After ultrasonic bath treatment and drying, phengite was hand-picked under a binocular microscope. An average of 60 to 80 inclusion-free grains was recovered from each sample in order to select the best grains for subsequent analysis. $^{40}Ar/^{39}Ar$ total fusion analyses were then carried out on selected single grains per sample. A detailed description of the sample procedure is given in Appendix 1B.

The primary goal was to select samples with only one foliation and phengite developed in S_2 (D_2) meets this criterion (samples 7CF3A, G-102, G-103, G-104; figs. 6A–6D) and allowed us to precisely date this event. However, most samples contain phengite that formed/deformed during more than one event. Samples having both S_1 and S_2 foliations were analyzed in order to determine the age of D_1 deformation (samples SM-45 and SM-47, respectively, figs. 6E and 6F). Samples with phengite oriented in the S_1, S_2 and S_3 foliations (sample SR-65b, fig. 5F) or S_2 and S_3 foliations (sample SR-65, fig. 6E) were analyzed in order to determine the age of the D_3 deformation.

The following four samples were selected to determine the timing of the D_2 deformation, since they only contained S_2 phengites. Sample 7CF3A (metacarbonate, table 7) yielded seven indistinguishable total fusion ages ranging from 55.60 ± 7.45 to 57.96 ± 2.50 Ma (Appendix 2B). We have calculated a weighted mean age of 57.2 ± 1.8 Ma (probability-P=0.95) based on all the total fusion ages (fig. 6A, Appendix 2A). In sample G-102 (calcschist, table 7), ten phengite total fusion ages range from 55.19 ± 11.11 to 63.03 ± 15.47 Ma and yield a weighted mean age of 56.7 ± 1.4 Ma (P=0.98) (fig. 6B, Appendices 2A and 2B), whereas in sample G-103 (calcschist, table 7) the thirteen total fusion ages record values from 54.79 ± 2.78 to 58.52 ± 1.71. The calculated weighted mean age is 56.32 ± 0.40 Ma (P=0.26), (fig. 6C, 2A). Eight total fusion ages from sample G-104 (metacarbonate, table 7) range from 55.15 ± 3.96 to 59.78 ± 2.46 Ma, with a weighted mean age of 58.01 ± 1.1 Ma (P= 0.44, fig. 6D, Appendices 2A and 2B). In addition, sample SM-47 (mica schist, table 7) shows the S_2 foliation cutting a relic S_1 foliation preserved inside microlithons defining rootless folds (fig. 3C). Eleven total fusion ages range from 55.79 ± 2.21 to 61.31 ± 4.97 Ma (Appendix 2B). Importantly, this sample contains crystals of two clearly-defined populations (S_1, S_2). The younger group (S_2) yielded an age of 56.8 ± 1.1 Ma (fig. 6F, Appendix 2A).

Sample SM-47 was specifically analyzed in order to determine the age of the S_1 foliation. The older group (S_1) records an $^{40}Ar/^{39}Ar$ weighted mean age of 59.4 ± 0.8 Ma. Sample SM-45 (quartz-mica schist, table 7) has the S_1 foliation oriented at a low angle to S_2 (fig. 3A). Six $^{40}Ar/^{39}Ar$ total fusion ages of phengites (mixed population S_1 and S_2) yielded values from 59.62 ± 1.36 Ma to 61.70 ± 1.99 Ma (fig. 6E, Appendix 2B)

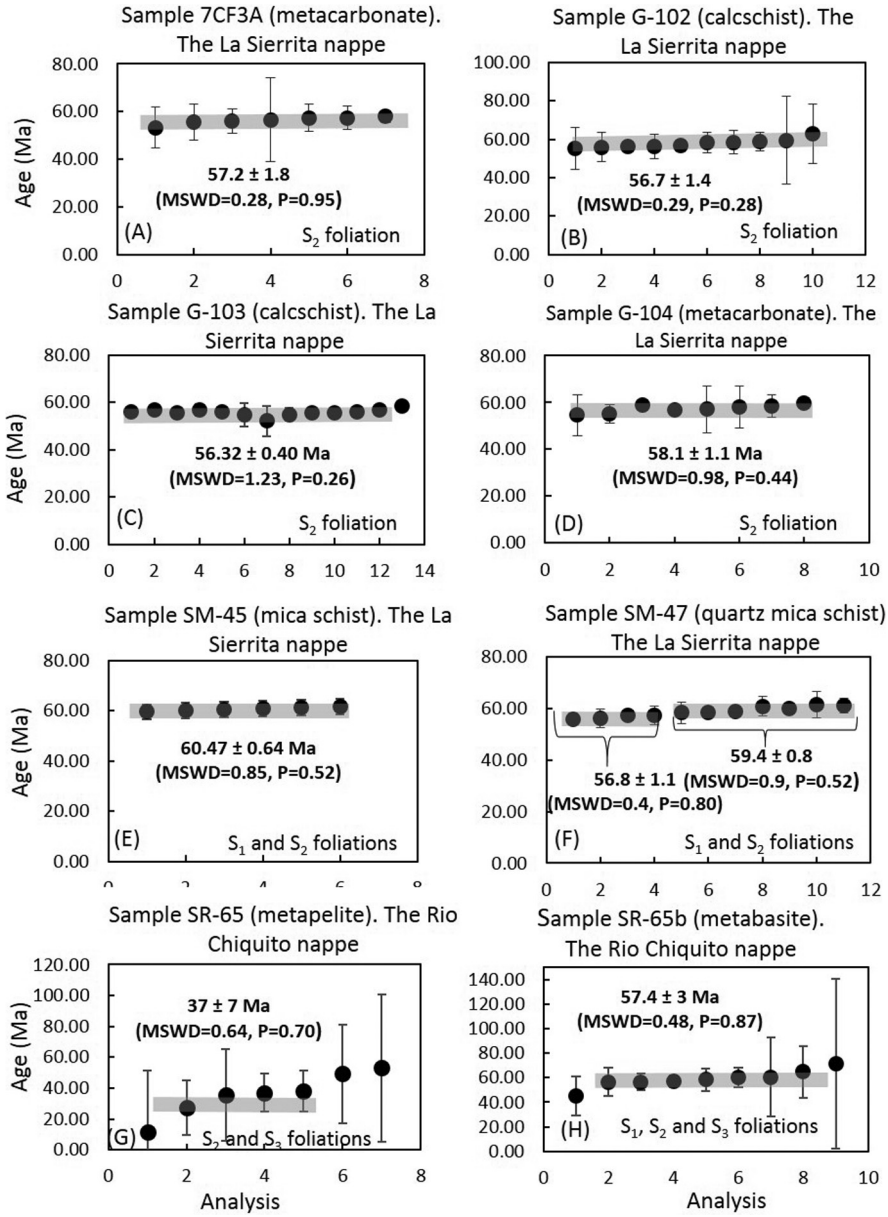

Fig. 6. $^{40}Ar/^{39}Ar$ total fusion ages (weighed means) from metasediments in the Trinidad dome, Escambray complex, Central Cuba.

and a weighed mean total fusion age of 60.47 ± 0.64 Ma (P=0.52), (fig. 6E, Appendix 2A). Although only a single population is evident, this is within error of the S_2 age recorded in sample SM-47 and is interpreted to date this event.

To determine the age of S_3 sample SR-65 (metapelite, table 7) was chosen because it shows a folded S_2 foliation and a new axial planar S_3 foliation defined by phengite developed in the fold hinges (fig. 3E). Unfortunately, this sample only contained very

TABLE 7

$^{40}Ar/^{39}Ar$ weighed mean ages for samples of the greenschist nappes in the Trinidad dome, Escambray complex, Cuba, with indication of rock types and mineral assemblages along S_1, S_2 and S_3 foliations

Sample	Mineral assemblage (*)	Total fusion age (weighed mean--Ma) (fig. 7)	Nappe	Rock type
7CF3A	S_2: Cal+Ph+Qtz+Chl+Ep+Ab	57.2 ± 1.8	La Sierrita	metacarbonate
G-102	S_2: Act+Cal+Ph+Chl+Qtz+Ep+Ttn+Ab	56.7 ±1.4	La Sierrita	calcschist
G-103	S_2: Act+Chl+Ph+Cal+Ep+Ab+Ttn	56.32 ± 0.40	La Sierrita	calcschist
G-104	S_2: Cal+Ph+Qtz	58.01 ± 1.1	La Sierrita	carbonate mica schist
SM-45	S_1: Ph+Chl+Grt S_2: Qtz+Chl+Ph+Ep+Grt+Hem+Ab	60.56 ± 0.66	La Sierrita	quartz mica schist
SM-47	S_1: Ph+ Gr S_2: Ab+Chl+Ph+Qtz+Ttn+Cal	56.8 ± 1.1 (group II) 59.4 ± 0.8 (group I)	La Sierrita	mica schist
SR-65	S_2:Ph+Ab+Chl+Ep+Cc+Qtz+Cal+Ttn+Hem S_3: Ph+Ttn+Chl+Ep	36 ± 7	Rio Chiquito	metapelite
SR-65b	S_1: Act+Ph S_2: Ph+Chl+Ep+Act+Ab S_3: Act+Ph +Ab	57.4 ± 3	Rio Chiquito	metabasite

(*) Mineral abbreviations after Whitney and Evans (2010).

small phengite crystals (125 mm) and, as a result, each individual total fusion age yielded a very poor precision due to the low argon beam signal measured in the mass spectrometer. This makes this data set extremely sensitive to blank correction and thus very unreliable. The seven total fusion ages fall in the interval between 11.28 ± 39.76 to 48.18 ± 32.04 Ma with a weighted mean age of 36 ± 7 Ma (P = 0.70), (fig. 6F, Appendices 2A and 2B). In a further attempt to constrain the timing of S_3, sample SR-65b (metabasite, table 7) was selected because it contains phengites oriented in three foliations (S_1, S_2 and S_3, fig. 3D). The nine total fusion ages for this sample range from 44.84 ± 15.85 to 64.83 ± 21.20 Ma (fig. 6H, Appendix 2B). The total weighted mean age is 57.4 ± 3 Ma (P=0.87) (fig. 6H, Appendix 2A).

P-T CONDITIONS AND PATHS

The pressure conditions have been estimated using the phengite barometer calibrations of Massone and Schreyer (1987), Massone and Szpurka (1997) and Simpson and others (2000). However since the calibrations imply the coexistence of phengite with the assemblage Qtz+Bt+Kfs+H_2O in the KMASH system, the calculated pressures are considered minimum estimates. Temperature estimations are more uncertain and difficult to calculate given the common presence of carbonate, which introduces unknown variables (XCO_2, XH_2O) in addition to P, and were considered to lie in the range of 300 to 400 °C according to the greenschist facies mineral assemblages coexisting with phengite. The estimated P-T path is hence general and only semi-quantitative for all greenschist-facies units. The extensive retrogression of the Monforte nappe prevents estimation of pre-retrogression stages. Retrograde

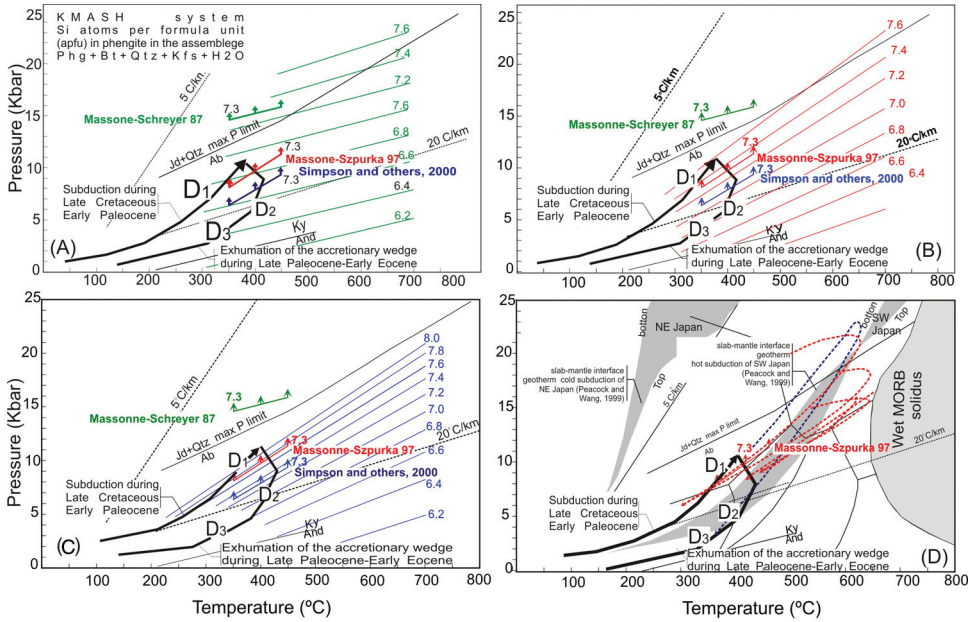

Fig. 7. P-T evolution of the greenschist-facies tectonic units in the Trinidad dome (in black). The paths are estimated according to Si-content in-phengite isopleths after (A) Massone and Schreyer (1987) in green, (B) Massone and Szpurka in red (1997) and (C) Simpsom and others in blue (2000). Note the maximum Si content of 7.3 apfu in phengite for each barometer calibration. (D) General path with indication of the facies scheme of Liou and others (2004), the wet MORB solidus (Peacock and others, 1994) and cold and hot slab mantle geotherms of NE and SW Japan respectively after Peacock and Wang (1999). For comparison, P-T trajectories of eclogite rocks from the Santi Spiritus dome (Schneider and others, 2004; Garcia Casco and others, 2006 and Stanek and others, 2006) and of eclogites from the Samaná complex of Escuder-Viruete and others (2006) are indicated as red and blue dashed lines, respectively.

greenschist-facies metamorphism in this nappe is however consistent with prograde metamorphism of the greenschist-facies units.

The Massone and Schreyer (1987) calibration predicts minimum peak pressures of about 15 kbar (at 400 °C) for the maximum Si content of phengite (Si = 7.3 apfu, sample SR-65, table 2), beyond the stability limit of albite (fig. 7A). This result indicates that this KMASH system calibration is not suitable for barometric estimations in complex natural systems. The calibrations of Massone and Szpurka (1997) and Simpson and others (2000) predict minimum peak pressures of 10 and 8 kbar (400 °C), respectively, both within the stability limit of albite (figs. 7B and 7C). Because these are minimum estimates of pressure, we consider that P-T conditions at peak pressure were in the range 9 to 11 kbar (at 350–400 °C). These conditions correspond to the high-pressure greenschist subfacies or the transition from HP greenschist to blueschist facies (Bousquet and others 1997), in agreement with the lack of blueschist facies assemblages in the low-T tectonic units.

It should be noted that the maximum Si phengite of 7.3 apfu corresponds to S_2 crystals. However, since relic D_1 phengite included within porphyroblasts has Si contents ranging from 6.32 to 6.88 apfu (maximum in the Yaguanabo nappe, table 2), and most phengites in the S_2 and S_3 planes have 6.60 to 6.87 and 6.52 to 6.80 apfu, respectively (fig. 5D), we consider that the peak pressure of 9 to 11 kbar based on the maximum Si phengite value corresponds to D_1 (that is, maximum Si phengite are D_1 crystals rotated into S_2). Indeed, S_2 and S_3 phengites are considered to be mixtures of

D_1+D_2 and $D_1+D_2+D_3$ crystals (that is, rotated/(re)crystallized grains). The minimum pressure estimates according to the full range of Si contents of $D_{2\text{-}3}$ phengite suggest a metamorphic evolution characterized by a steady pressure decrease as exhumation proceeded (fig. 7).

Important observations for estimating P-T evolution are the local growth of biotite at S_2 rims of chlorite (the Rio Chiquito nappe) and the orientation of magnesio-hornblende, along with actinolite, in S_2 matrix minerals (the Rio Chiquito nappe). These features suggest slight heating during the initial stage of decompression (D_2), at least in the Rio Chiquito nappe (fig. 7D). The presence of hematite in samples with magnesio-hornblende has been used to estimate temperatures between 400° up to 480 °C in mediun-grade rocks (Otsuki and Bano, 1990). However it is unlikely that the temperature in this case exceeded 450 °C given the lack of extensive recrystallization in the lower epidote-amphibolite facies. The mineral assemblage in the metabasites consists of Mg-hornblende, actinolite, epidote, chlorite, phengite, albite ± biotite ± hematite. It represents a transition from the greenschist to the epidote-amphibolite facies. The plagioclase is almost pure albite (X=0.98) in composition and coexists with chlorite and epidote. Biotite has low Ti (max 0.13) content indicative of low temperatures (below 500 °C, Henry and others, 2005). Garnet is present in pelitic rocks according to bulk composition. These facts indicate a temperature less than 450 °C (for example Andersen and others, 1998). On the other hand, the HP rocks of the Monforte nappe underwent retrograde metamorphism in the lower part of the blueschist, epidote amphibolite and greenschist facies (fig. 7D).

Calcite twinning related to D_3 in metacarbonates from all nappes indicates temperatures in the range of 150 to 300 °C (Despaigne-Díaz and Caceres Govea, 2009b). At this period, retrogression was still taking place as the nappe stack was consolidated. The lowest Si value in S_3 phengite from metapelites of the Rio Chiquito nappe (Si = 6.52 apfu, table 2) gives a minimum pressure of about 5 kbar following the Massone and Szpurka (1997) and Simpson and others (2000) barometers (figs. 7B and 7C), in agreement with progressive decompression and cooling.

In figure 7D we present the estimated P-T path of the greenschist units incorporating the geothermal gradients of Peacock and Wang (1999) calculated along the slab/mantle interface for subduction of cold and warm slabs in NE and SW Japan. The path followed by these units are closer to warm subduction, suggesting that the subducted oceanic lithosphere was relatively young, but did not melt at relatively moderate pressures, contrary to what has been observed in Eastern Cuba where a young slab underwent partial melting during the earliest subduction stage at *ca.* 120 Ma (García-Casco and others, 2008b; Lazaro and others, 2009, Blanco-Quintero, and others 2010, 2011). This thermal evolution indicates refrigeration of the subduction system due to continued subduction during the Cretaceous (120–70 Ma). Figure 7D also shows the P-T paths of Schenider and others (2004), Stanek and others (2006), and García-Casco and others (2006) for the structurally upper Unit III of the Sancti Spiritus dome of the Escambray complex and of Escuder-Viruete and Pérez-Estaún (2006) and Escuder-Viruete and others (2011b) for the correlated Samaná complex in the Dominican Republic. The units in the Trinidad dome followed a similar path but at lower pressures, indicating subduction to shallower depths.

DISCUSSION

Interpretation of the $^{40}Ar/^{39}Ar$ data

In this study, geochronological information is supported by petrological and microstructural relationships of mineral assemblages. Although precise closure temperature of a mineral depends on grain size, cooling rates and chemical composition, closure temperatures for phengites generally range from 350 to 450 °C for the

$^{40}Ar/^{39}Ar$ system (Purdy and Jaeger, 1976; Kirschner and others, 1996, McDougall and Harrison, 1999). Since temperature during greenschist-facies metamorphism in the studied units was below the activation temperature for Ar diffusion in phengitic mica (fig. 7) we consider that our $^{40}Ar/^{39}Ar$ ages correspond to the metamorphic growth of phengites (D_1) near to peak metamorphic conditions (D_2) and further retrogression and/or recrystallization during D_3.

The age of D_1 deformation is constrained by the weighted mean ages from sample SM-47 (with two distinct phengite populations) and sample SM-45 from the La Sierrita nappe, together with sample SR-65b from the Rio Chiquito nappe. S_1 phengites represent a prograde path during peak metamorphism. The weighted mean ages obtained from samples SM-47 and SM-45 are 59.4 ± 0.8 Ma and 60.47 ±0.44 Ma, respectively (figs. 6E, 6F, and 6H). Sample SR-65b yielded an age of 57.5 ± 3 Ma. As this sample contains a wider mixture of phengite populations (S_1, S_2 and S_3), we consider peak metamorphism in the greenschist facies during D_1 is best reflected by the results of samples SM-45 and SM-47, corresponding to the Middle Paleocene.

The lack of zoning in S_1 phengites indicates no chemical readjustment during subsequent deformation. We argue that the D_2 thermal event was of insufficient magnitude or duration to induce resetting of the $^{40}Ar/^{39}Ar$ system and the S_1 micas retained their older ages (figs. 6E and 6F). All these facts indicate that the age of S_1 phengites reflects the timing of D_1 deformation and represents phengite growth during prograde metamorphism and hence can be related to this deformational event.

The age of D_2 deformation was obtained from samples exhibiting only the S_2 foliation, together with sample SM-47 that contained both S_2 and S_1. The age spectrum ranges between 56.32 ± 0.40 M and 57.4 ± 3 Ma (figs. 6A, 6B, 6C and 6D). According to microstructures (fig. 4), the S_2 phengites also lack zoning. We exclude any contribution from excess Ar in this case, as this would invariably lead to variable total fusion ages depending on the amount of excess argon in each crystal (figs. 6A, 6B, 6C and 6D). We consider that the results from sample G-103 (56.2 ± 0.4 Ma, fig. 6C) give the best estimate of the age of S_2 corresponding to the Upper Paleocene. This age should correspond to the onset of cooling after a short-lived heating event related to D_2 deformation and indicate that the temperature increase during D_2 occurred over a short time period. Retrogression of garnet to chlorite occurs along the S_2 foliation in mica schist from the la Sierrita nappe (fig. 4A), also indicating cooling at this stage. We suggest that the age of the S_2 phengites most likely reflects cooling close to the phengite closure temperature.

The timing of D_3 deformation is less precise. The S_3 foliation planes are "contaminated" with phengites from two other populations (S_1 and S_2) and are indistinguishable. P-T and microstructural data show that phengites reoriented/recrystallized at temperatures of about 300 °C and record cooling after peak metamorphism. As observed in figure 6G, the spectrum for sample SR-65 yielded no reliable age. In this sample, a well-developed S_2 foliation caused folding of mica flakes and an S_3 surface developed in the D_3 fold hinges (fig. 3E). Locally, recrystallization of micas is observed. The age of 36 ± 7 Ma is likely to be younger than phengites in the fold limbs or be influenced by recrystallization (Wijbrans and McDougall, 1986). Hence we consider this age to be spurious and therefore of no geological significance. However, sample SR-65b shows a more consistent spectrum and the weighted mean age of 57.4 ± 3 Ma overlaps the age for D_2 deformation. We postulate that D_3 deformation must be younger than 60 Ma and older than 50 Ma, corresponding to the Late Paleocene-Early Eocene. Geological evidence supports this age estimation, as the first debris of HP rocks from the Escambray occur in 45 to 50 Ma conglomerates from neighboring

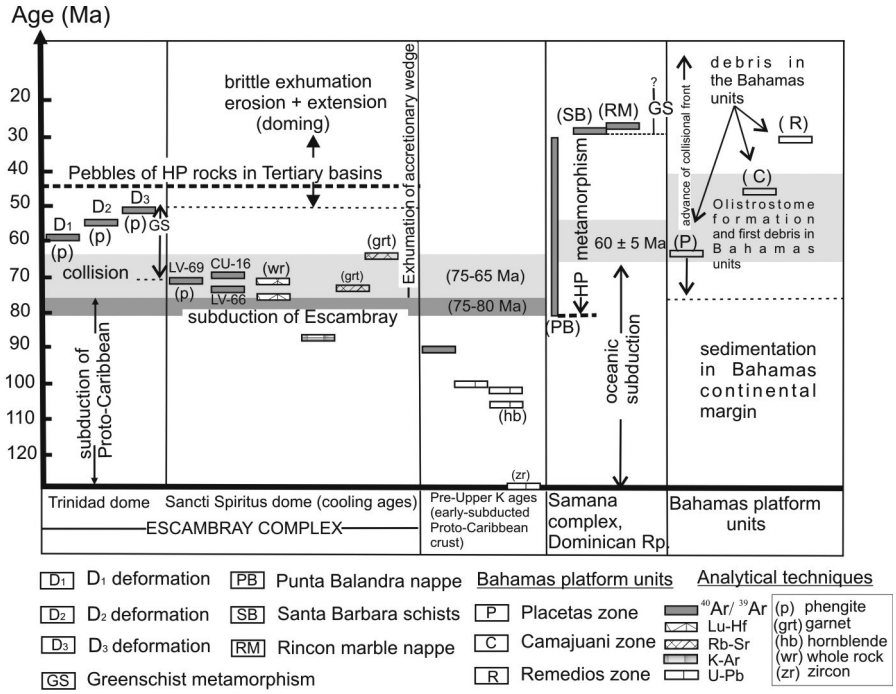

Fig. 8. $^{40}Ar/^{39}Ar$ isotopic data from the Trinidad dome (this study) and compilation of published geochronological data for the Escambray and Samaná complexes and the Bahamas platform (see text for discussion). Data from the Sancti Spiritus dome (LV-66, LV-69 and CU-16) are from Schneider and others, (2004). Additional data for the Sancti Spiritus dome from Somin and Millán (1981), Hatten and others (1988, 1989), Somin and others (1992), Stanek and Maresh (2007). Data from the Samaná complex from Escuder-Viruete and others (2011a). Age data for the Bahamas units from Iturralde-Vinent and others (2008).

Tertiary basins (Kancthev, 1978, fig. 8), yielding a period of 6 Ma from 56 to 50 Ma for the development of D_3.

It should be noted that ductile deformation associated with greenschist-facies metamorphism in the Trinidad dome took place in intervals of 5 to 6 million years apart, the first occurring shortly after burial. Our results indicate the units of the Trinidad dome were still undergoing greenschist-facies metamorphism and exhumation during the Late Paleocene. These units were ascending to the surface along thrust faults as they were accreted and deformed in the collisional wedge.

Structural Development and Mechanisms of Exhumation

The Escambray accretionary complex formed and was exhumed from the latest Cretaceous to Tertiary. Our P-T data from the Trinidad dome indicate the greenschist-facies units were buried to 35 km depth and formed an imbricated thrust stack (the highest-grade Monforte unit on top of the tectonic pile). Peak metamorphism of the greenschist-facies units occurred at 11 kbars and 400 °C during D_1 (figs. 7B and 7C).

The structural development of the Trinidad dome can be seen as a process of three syn-metamorphic deformations (D_1, D_2 and D_3) and two deformations (D_4-D_5) under a brittle-ductile and brittle environment at sequentially shallower crustal levels. Subduction of the sedimentary pile (Caribeana terrane of García-Casco and others, 2008a) started in the structurally upper Unit III at about 80 to 70 Ma based on peak and cooling ages of HP rocks of the Sancti Spiritus dome (Schneider and others, 2004;

García-Casco and others, 2006; Stanek and others, 2006; Stanek and Maresh, 2007) and lasted until about 60 Ma according to our isotopic data (D_1, figs. 9A and 9B) from the Trinidad dome (see also Stanek and others, 2006). Eclogites and metabasites intercalated with the metasediments of the Monforte nappe in the Trinidad dome are strongly retrograded, but HP metamorphism in the eclogite facies likely occurred in the Late Cretaceous-Paleocene (D_1 deformation) when similar rocks of the Sancti Spiritus dome were subducted. Hence, this HP unit was buried before the greenschist-facies nappes were dragged down and metamorphosed (figs. 9A and 9B). Eclogites with different pre-eclogitic histories in the Sancti Spiritus dome (one variety interlayered with metasediments and the other occurring as tectonic blocks within serpentinite melange), were both incorporated in the subduction zone and subsequently underwent a similar deformation history (Schneider and others, 2004).

There are several pieces of evidence that allow correlation of D_2 deformation with onset of exhumation of the greenschist-facies units (the La Sierrita, Yaguanabo and the Rio Chiquito nappes) in the Middle Paleocene (at 56.32 ± 0.4 Ma), including: 1) parallelism of S_2 foliation with strongly-sheared serpentinite layers/bodies along main tectonic contacts, arguing for exhumation along major faults of hanging wall mantle and/or subducted ophiolitic material; 2) tectonic repetition of the sequence of schist, calcschist, metachert, metapelite and metabasite at outcrop scale, indicating thrust stacks and underthrusting; and 3) the greenschist-facies imprint on the eclogitic Monforte nappe, arguing for emplacement of deeply subducted material on top of the shallower nappes.

In figure 9, we summarize the tectonic evolution of the Trinidad dome. Shortly after peak metamorphism, Monforte nappe started to be exhumed (D_2) from 75 to 60 Ma when the La Sierrita, Yaguanabo and the Rio Chiquito nappes were still sinking (D_1) in the subduction zone (fig. 9B). The only evidence of retrogression in the greenschist-facies units comes from the La Sierrita nappe, where garnets are replaced by retrograde chlorite (fig. 4A). This indicates that the La Sierrita nappe was the deepest of the greenschist-facies units in the subduction zone and reached slightly higher grade (fig. 9B).

The short-lived heating event during D_2 deformation, with no significant pressure drop requires comment (fig. 7). Stanek and others (2006) suggested that continuous arrival of continental units in a subduction zone cause thickening of the accretion zone and a decrease of the subduction angle. This thickening event may cause the subduction zone to choke, leading to local heating; in the Trinidad dome example it was associated with D_2 deformation. This short-lived heating event during D_2 reached lower epidote-amphibolite facies though recrystallization was incomplete (fig. 7D). The high Si content of S_2 phengites [6.55–7.3 apfu, table 2; the higher value (7.3) interpreted as a rotated D_1 crystal] confirms that metamorphism took place under relatively high pressures (8–9 kbar and 400–450 °C, figs. 7A and 7D). This temperature increase can be related to the emplacement of the HP rocks of the Monforte nappe on top of the Rio Chiquito nappe, pointing to a similar time for retrogression of the Monforte nappe in the lower part of the epidote-amphibolite facies (fig. 7D). Millán (1997b) previously reported that eclogite-facies rocks of tectonic Unit III underwent blueschist facies retrogression, and related this overprinting to the low-grade, high-pressure metamorphism of Unit II.

The nappe structure was consolidated by 50 Ma (Late Paleocene-Early Eocene) during D_3 deformation. At this stage, the units were already inverted in terms of the position they occupied in the subduction zone. Exhumation unroofed the HP Monforte nappe on top of the lower grade units (fig. 9D), in agreement with the structure of other accretionary complexes (Kimura and others, 1996; Agard and others, 2001, 2009; Stanek and others, 2006; Escuder-Viruete and others, 2011a, 2011b). Kinematic

indicators indicate tectonic movement to the north and northeast during exhumation (fig. 2). Temperatures decreased as the units were thrust upwards and dropped from 300 to 150 °C, with pressures dropping down to 5 kbar (fig. 7D).

From 50 Ma onwards, exhumation continued under a brittle-ductile and brittle regime with formation of en-echelon and extension veins and brittle structures. In the Trinidad dome, a series of open folds with vertical axial planes relate to the domal structure and were linked to a regional S_4 spaced cleavage formed during D_4 deformation.

The last deformation (D_5) took place under a brittle regime after the nappe stack was consolidated. Strike-slip faults and low-angle normal faults occur along the southwestern margin of the Trinidad dome locally associated with steep axial planar folds. The present-day shape and structure of the Escambray led Draper (2001) to hypothesize that it was a core complex, similar to what has been suggested for the nearby Pinos Terrane, (García-Casco and others, 2001). The antiformal structure, the domal pattern foliations (see also Millan and Somin, 1985) and the low angle normal faults along the border of the Trinidad dome indicate the unroofing. Extension was important during the Tertiary and caused the opening of the Trinidad basin between the two domes (fig. 2). Stanek and others (2006) identified a mylonitic greenschist-facies shear zone between the Mabujina amphibolite and the Yayabo unit (Escambray complex) in the Sancti Spiritus dome, and suggested it acted as a main detachment between the Escambray accretionary complex and the overlying arc complex. Even though this shear zone has not been identified in the study area we do not exclude the possibility that these low-angle normal faults led to the subsequent evolution of a major extensional geometry (detachment fault) at a regional scale.

The first erosional debris of HP rocks from the Escambray complex is recorded in 45 to 50 Ma conglomerates from nearby basins (Kantchev, 1978), marking the time when the Escambray was unroofed and deeply eroded.

Thrusting as the sole mechanism is not enough to exhume rocks buried to depths greater than 30 km and a combination of several mechanisms is required to explain the exhumation of HP rocks (Platt, 1993). The calculated exhumation rate for the Escambray ranges from 2 to 4.5 mm/yr, and is consistent with exhumation rates of serpentinite or muddy-shaly weak melanges containing blocks of subducted oceanic and continental crust (see fig. 9A of Agard and others, 2009). We suggest that the P-T trajectories followed by the Trinidad dome units, combined with erosion and the activation of normal faults during the $D_{4\text{-}5}$ deformation phases, indicates a combination of several mechanisms in the exhumation of the accretionary complex. The upper boundaries of the complex are marked by normal low-angle faults that are more abundant toward the dome rim, which indicates that extension was more important than thrusting at the surface. Our results show that underthrusting and crustal thickening took place first, associated with subduction/collision of the Escambray complex, followed by extensional tectonics.

Geodynamic Implications

In this work, we consider the Escambray as part of the sedimentary pile of the Caribeanan terranes (offshore of the Maya block), and that continued subduction of the Proto-Caribbean oceanic lithosphere below the Caribbean plate took place during the Cretaceous (Pindell and Kennan, 2009). Subduction/collision of the Escambray complex started in the Late Cretaceous (~75–70 Ma, figs. 9A and 9B).

Fig. 9 (continued). and NNE directed thrust faults. (D) D_3 nappe stacking, decompression, syn-orogenic basin formation and debris in the Bahamian units. (E) $D_{4\text{-}5}$ are post-metamorphic and reflect the final brittle-ductile and brittle exhumation stage of the Escambray development, the final domal shape and the present time configuration of the Cuban fold and thrust belt.

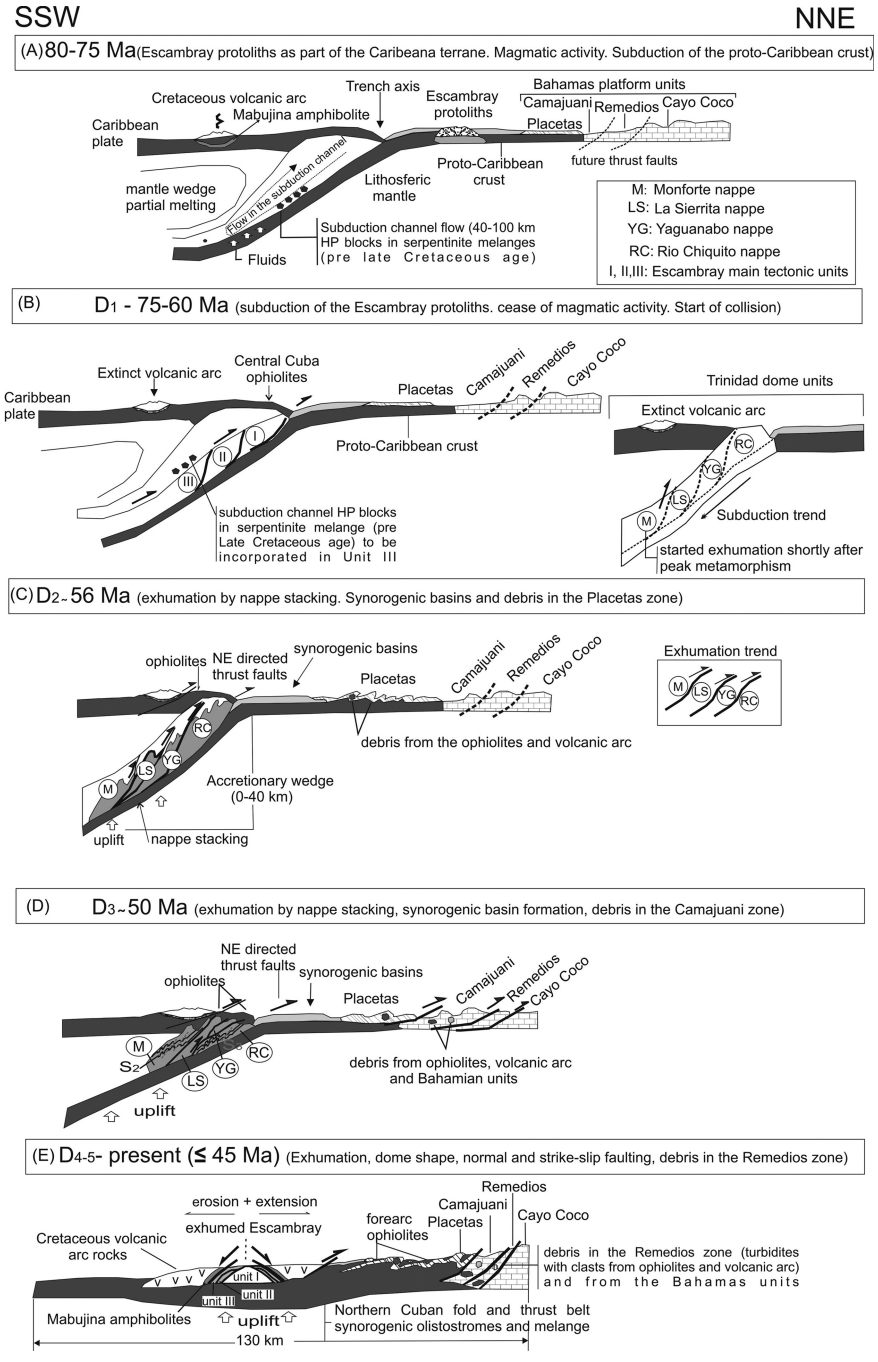

Fig. 9. Schematic tectonic model for the Escambray and the Trinidad dome based on interpretation of structural, tectonic, petrologic and isotopic data, showing the processes of subduction-accretion-exhumation in the accretionary wedge and the structural evolution until final collision with the Bahamas platform. The main tectono-metamorphic stages D_1, D_2 and D_3 are specified. (A) Escambray protoliths. (B) D_1 subduction and prograde HP metamorphism. (C) D_2 nappe stacking and decompression, retrograde metamorphism

The timing of collision with the Bahamas platform needs to be discussed, as it has several implications for the evolution of the Cuban fold and thrust belt and Caribbean geology. Some authors have equated the Escambray complex with subduction of the Bahamas platform and arc-continent collision (Schneider and others, 2004; Stanek and others, 2006). Stanek and others (2006) concluded that thrusting of the accretionary complex and the volcanic arc onto the Bahamas platform took place around 65 Ma. Likewise, Escuder-Viruete and others (2011b) considered the building of the nappe pile of the Samaná complex, Dominican Republic, to be the result of oblique subduction of the Proto-Caribbean Ocean and subduction of the Bahamas platform. On the other hand, there is geological evidence for a Bahamas platform–arc collision starting in the Paleogene (Iturralde-Vinent, 1994, 1998a; Iturralde-Vinent and others, 2008; Garcia Casco and others, 2008a) and continuing through to the Late Eocene. The first debris of olistrostomic syn-tectonic formations (recording the Caribbean plate-Bahamas collision) in the more distal Bahamas unit (Placetas) is of early Paleocene age (fig. 9C) and consists of ophiolite-derived blocks and Cretaceous volcanic arc rocks. As the deformation front moved northeast, syn-tectonic debris contributed to Middle to Late Eocene deposits as far east as the Remedios zone (fig. 9E). In figure 8, we summarize age data from the Escambray and Samaná complexes and the Bahamas units. The Escambray ages demonstrate exhumation occurred from 70 Ma until the Late Paleocene-Early Eocene, in contrast with deformation of the Bahamas platform units that only occurred since the Paleocene (Iturralde-Vinent and others, 2008; Garcia Casco and others, 2008a; Van Hinsbergen and others, 2009). Subduction/collision in the Samaná complex started at 65 ± 5 Ma (fig. 8), shortly after subduction of the Escambray. The thermal gradient of the greenschist-facies units of the Trinidad dome was colder compared with the Samaná complex, in agreement with the fact that the eclogites of Samaná complex and Escambray Unit III subducted before Escambray Unit I (fig. 7D). The younger ages in the Samaná complex suggest that drifting of the Caribbean plate to the northeast continued by normal subduction of the Proto-Caribbean until its final collision with the Bahamas platform in the Eocene. The whole complex was transected by Oligocene and younger strike-slip faults associated with the Septentrional fault zone (Escuder-Viruete and others 2011a, 2011b).

The collision of the sedimentary piles belonging to the Caribeanan terranes with the Bahamas platform (including the Escambray in the Cuban segment) took place shortly after 45 to 50 Ma when the Escambray nappe stack reached the surface and was deeply eroded. Paleogeographic reconstruction of the Cuban fold belt demonstrates a more southerly position of original units before thrusting and shortening in the Late Cretaceous, implying the Escambray and Bahamas were initially far apart (Iturralde-Vinent and others, 2008; García-Casco and others, 2008a). The Escambray was incorporated into the Cuban fold and thrust belt in response to southwest-northeast compression from the Late Cretaceous onwards and before the Late Eocene arc-continent collision between the Caribbean and North American plates (Iturralde-Vinent and others, 2008).

At least from the Early Eocene, a significant kinematic change affected the entire northern Caribbean region. Relative motion of the Caribbean shifted to a more eastward direction with respect to North America (Pindell and others, 2005, 2006). In the Late Eocene, Cuba was finally sutured with the Bahamas platform and sedimentation resulted in the infill of post-orogenic basins (Puscharovsky and others, 1989; Saura and others, 2008; Iturralde-Vinent and others, 2008).

CONCLUSIONS

Our results add to the previous $^{40}Ar/^{39}Ar$ cooling ages of high-grade rocks (eclogites and blueschists) of the structurally higher Units II and III of the Escambray

complex, allowing for an evaluation of the complete time interval from subduction/collision to final exhumation of the accretionary complex. The metamorphic evolution of tectonic units during three major ductile deformation phases (D_1, D_2, and D_3) was related to subduction and collision-exhumation of the accretionary wedge from the Late Cretaceous to the Early Eocene. Peak metamorphism of the units took place during D_1 deformation in the Late Cretaceous Middle Paleocene (75–60 Ma). D_2 deformation was contemporary with exhumation of the tectonic pile and corresponds to the superposition of eclogitic metamorphic units (Monforte nappe in the Trinidad dome) over less metamorphosed nappes in the Escambray. This deformation produced NNE emplacement of the nappes that were progressively incorporated into the thickening accretionary wedge during the Middle Paleocene (~56 Ma). D_3 structures formed under a ductile to brittle-ductile regime, indicating exhumation in the accretionary wedge continued until the Late Paleocene, and may have lasted until the Early Eocene (56–50 Ma).

The exhumation of the Trinidad dome occurred in two main episodes: 1) ductile exhumation with accretion and deformation in the accretionary wedge from 56 to 50 Ma during $D_{2\text{-}3}$ deformation and, 2) brittle-ductile and brittle deformation from 50 Ma onwards, associated to doming, post-metamorphic strike-slip and normal faults leading to unroofing and erosion associated with the $D_{4\text{-}5}$ deformations.

Since the Early Eocene, the Escambray has been deeply eroded and uplifted and the deformation front represented by the allocthonous ophiolite and Cretaceous volcanic rocks shifted towards the NE until final collision with the Bahamas platform that sutured the fold belt. The deformational events in the Trinidad dome lasted from 75 to 50 Ma and record 25 million years of intraoceanic subduction/collision/exhumation in the northern Caribbean, documenting deformation and metamorphism along the leading edge of the Caribbean plate.

ACKNOWLEDGMENTS

Ana Ibis Despaigne-Diaz wishes to acknowledge research funds from a MAEC-AECI fellowship of the Spanish Cooperation Agency and from project BTE 2002-010011 “Terrenos metamórficos en el margen septentrional del Caribe (Cuba)” of the Ministerio de Ciencia, Tecnología y Medio Ambiente, Spain, for analytical support and field work assistance. We thank Dr. Jorge Cobiella from the University of Pinar del Rio, Cuba, Grenville Draper, and Darrel Cowan for critical reviews that helped to improve the manuscript. We also thank Dr. Martin Meschede and Dr. Heiko Hueneke from Greifswald University, Germany, for initial financial support. This work was carried out during the tenure of a Visiting Fellowship at Curtin University, Australia, to the senior author from the Institute for Geoscience Research (TIGeR). This is a contribution to IGCP project 546 “Subduction zones of the Caribbean”.

APPENDIX 1A

Analytical Techniques and Procedures for EPMA Analysis

Mineral compositions were obtained using two instruments at the University of Granada. A CAMECA SX-100 microprobe with WDS, was operated at 15 KV and 15 nA, pixel size 4–8 μm, counting time 30 ms. Synthetic SiO_2, Al_2O_3, $MnTiO_3$, Fe_2O_3, MgO, TiO_2, $BaSO_4$ and natural diopside, albite, and sanidine were used as calibration standards. A Leo 1430 VP EM equipped with a microanalysis energy disperse system RX (EDS) Inca 350v.17 from Oxford Instruments was also utilised. Samples were processed at 30 KV and 50 s. Spectra were acquired with a current range varying from 0-20 KeV and a resolution of 10eV/Ch. Resolution of X-Ray maps are lower up to 20 KeV/Ch.

X-Ray images were obtained with the CAMECA SX-100 microprobe at the University of Granada with operating conditions of 50 and 100 nA. The images were processed with ***Imager*** software (Torres Roldán and García Casco, unpublished) and consist of X-Ray signals of Kα lines of the elements, except Ba (Lα lines) or element ratios expressed as colors or counts/n/nA/s, corrected for 3 μs dead time. Images were processed

(mask out) to avoid defects in the thin section. Masks of minerals were overlain onto a grey scale base image layer obtained in CAMECA SX-100 (back scattered electron image, BSE Z).

Amphibole compositions followed the scheme of Leake and others (1997). Garnet was normalized to 8 cations and 12 oxygens, and Fe^{3+} calculated by stoichiometry. Epidote, and Plagioclase were normalized to 8 cations and 12.5 oxygens and 5 cations and 8 oxygens, respectively and $Fe_{total}=Fe^{3+}$. Micas and Chlorite were normalized to 22 and 28 oxygens, respectively, and $Fe_{total}=Fe^{2+}$.

APPENDIX 1B

Sample Procedure for $^{40}Ar/^{39}Ar$ Dating

Samples were loaded into aluminium discs containing eight wells 1.9 cm in diameter and 0.3 cm deep. These wells were bracketed by smaller wells that included Fish Canyon sanidine (FCs) used as a neutron fluence monitor for which an age of 28.294 ± 0.036 Ma (1σ) was adopted (Renne and others, 2011). The discs were Cd-shielded (to minimize undesirable nuclear interference reactions) and irradiated for 40 hours in the US Geological Survey nuclear reactor (Denver, USA) in a central position. The mean J-value computed from standard grains within the small pits is 0.009006 (0.13%) determined as the average and standard deviation of J-values of the small wells for each irradiation disc. Mass discrimination was monitored using an automated air pipette and provided a mean value of 1.006312 to 1.006341 per dalton (atomic Mass unit) relative to an air ratio of 298.56 ± 0.31 (Lee and others, 2006). The correction factors for interfering isotopes were $(^{39}Ar/^{37}Ar)_{Ca} = 7.30x10^{-4}$ (±11%), $(^{36}Ar/^{37}Ar)_{Ca} = 2.82x10^{-4}$ (±1%) and $(^{40}Ar/^{39}Ar)_{K} = 6.76x10^{-4}$ (±32%).

The $^{40}Ar/^{39}Ar$ analyses were performed at the Western Australian Argon Isotope Facility at Curtin University. For each sample, a series of single crystals of phengite were analyzed in one heating step (total fusion) using a 110 W Spectron Laser System, with a continuous Nd-YAG (IR; 1064 nm) laser rastered over the sample for 1 minute to ensure an homogenously distributed temperature. The gas was purified in a stainless steel extraction line using two SAES AP10 getters, a GP50 getter and a liquid nitrogen condensation trap. Ar isotopes were measured in static mode using a MAP 215-50 Mass spectrometer (resolution of ~500; sensitivity of $4x10^{-14}$ mol/V) with a Balzers SEV 217 electron multiplier mostly using 9 to 10 cycles of peak-hopping. The data acquisition was performed with the Argus program written by M.O. McWilliams and ran under a LabView environment. The raw data were processed using the ArArCALC software (Koppers, 2002) and the ages have been calculated using the decay constants recommended by Renne and others (2010). Blanks were monitored every 3 to 4 steps and typical ^{40}Ar blanks range from 1×10^{-16} to 2×10^{-16} mol. Ar isotopic data corrected for blank, mass discrimination and radioactive decay are given in Appendices 2A and 2B. Individual errors in Appendices 2A and 2B are given at the 1σ level.

APPENDIX 2A

$^{40}Ar/^{39}Ar$ data of all studied samples. All analyses correspond to phengite

Sample	Grains per sample	Weighted mean total fusion ages	MSWD	P	^{39}Ar%	Normal Isochron*	Inverse Isochron*	K/Ca 2σ
7CF3A	7	57.20 ± 1.80	0.28	0.95	100	58.34 ± 3.48	58.52 ± 3.47	0.3 ± 7
G-102	10	56.7 ± 1.4	0.29	0.98	100	57.00 ± 1.91	56.30 ± 2.41	0.08±0.33
G-103	13	56.32 ± 0.40	1.23	0.26	92.7	56.83 ± 1.32	55.38 ± 1.58	0.67±0.23
G-104	8	58.1 ± 1.1	0.98	0.44	100	58.30 ± 2.59	58.23 ± 2.25	0.48 ±0.5
SM-45	6	60.47 ± 0.64	0.85	0.52	100	56.30 ± 7.87	55.89 ±8.25	8.± 1723
SM-47	11	59.4 ± 0.8	0.9	0.52	62.5	60.49 ± 2.84	56.73 ± 4.35	1.3 ± 3.4
		56.8 ± 1.1	0.4	0.80	62.5	60.49 ± 2.84	56.73 ± 4.35	1.3 ± 3.4
SR-65	7	36.7 ± 7	0.64	0.80	100	40.19 ± 13.29	39.57 ± 12.57	0.02±0.1
SR-65b	9	57.4 ± 3	0.48	0.87	100	56.64 ± 3.91	56.75 ± 3.85	20 ± 46

* Weighed mean age in (Ma). Sample SM-47 gives two distinct age groups (see text for discussion).

APPENDIX 2B

$^{40}Ar/^{39}Ar$ total fusion ages of individual grains from each sample

Sample	Age of each grain ± 2σ Ma												
	1	2	3	4	5	6	7	8	9	10	11	12	13
7CF3A	55.60±7.45	57.96±2.50	56.02±4.95	57.44±5.02	53.26±8.55	57.27±5.72	56.60±17.52						
G-102	56.21±6.40	58.29±5.41	58.32±6.07	56.62±0.09	58.71±4.78	56.07±0.78	55.88±7.55	55.19±11	59.35±22.97	63.03±15.47			
G-103	56.16±1.45	56.86±0.67	55.66 ±0.90	56.92±2.51	55.93±2.04	54.70±5.03	52.10 ±6.42	54.79±2.68	55.66±0.90	55.69±2.16	56.16±1.45	56.85±0.67	58.52±1.71
G-104	58.50±4.83	54.56±8.53	56.95±1.92	55.15±3.96	58.81±1.79	57.19±10.01	59.78±2.46	58.28±9.04					
SM-45	60.08±1.34	59.62±1.36	60.55±1.17	60.96±1.71	61.33±2.54	61.70±1.99							
SM-47	56.11±3.67	55.79±2.21	57.04±1.42	57.23±3.70	58.26±4.13	58.40±1.89	58.72±1.94	60.76±2.91	59.77±1.14	61.31±4.97	61.96±2.80		
SR-65	35.83±29.72	49.18±32.04	11.28±39.76	52.93±47.68	37.09±12.16	38.15±13.35	27.26±13.90						
SR-65b	64.83±21.20	44.84±15.85	57.23±4.71	56.58±6.54	60.01±7.01	58.56±9.19	60.51±32.07	56.56±11.64	71.11±69.21				

REFERENCES

Agard, P., Jolivet, L., and Goffé, B., 2001, Tectonometamorphic evolution of the Schistes Lustrés complex: implications for the exhumation of HP and UHP rocks in the Western Alps: Bulletin Société Géologique de France, v. 172, n. 5, p. 617–636, http://dx.doi.org/10.2113/172.5.617

Agard, P., Yamato, P., Jolivet, L., and Burov, E., 2009, Exhumation of oceanic blueschists and eclogites in subduction zones: Timing and mechanisms: Earth Science Reviews, v. 92, n. 1–2, p. 53–79, http://dx.doi.org/10.1016/j.earscirev.2008.11.002

Andersen, T. B., Berry, H. N., IV, Lux, D. R., and Andresen, A., 1998, The tectonic significance of pre-Scandian $^{40}Ar/^{39}Ar$ phengite cooling ages in the Caledonides of western Norway: Journal of the Geological Society, London, v. 155, p. 297–309, http://dx.doi.org/10.1144/gsjgs.155.2.0297

Blanco-Quintero, I. F., Rojas-Agramonte, Y., García-Casco, A., Kröner, A., Mertz, D. F., Lázaro, C., Blanco-Moreno, J., and Renne, P. R, 2011, Timing of subduction and exhumation in a subduction channel: Evidence from slab melts from La Corea Mélange (eastern Cuba): Lithos, v. 127, n. 1–2, p. 86–100, http://dx.doi.org/10.1016/j.lithos.2011.08.009

Blein, O., Guillot, S., Lapierre, H., Mercier-de-Lépinay, B., Lardeaux, J. M., Millán Trujillo, G., Campos, M., and García, A., 2003, Geochemistry of the Mabujina Complex. Central Cuba: Implication on the Cuban Cretaceous arc rocks: The Journal of Geology, v. 111, n. 1, p. 89–101, http://dx.doi.org/10.1086/344666

Boschman, L. M., Van Hinsbergen, D. J. J., Torsvik, T. H., Spakman, W., and Pindell, J. L., 2014. Kinematic reconstruction of the Caribbean region since the Early Jurassic: Earth-Science Reviews v. 138, p. 102–136, http://dx.doi.org/10.1016/j.earscirev.2014.08.007

Bousquet, R., Goffé, B., Henry, P., Le Pichon, X., and Chopin, C., 1997, Kinematic, thermal, petrological model of the Central Alps: Lepontine metamorphism in the upper crust and eclogitization of the lower crust: Tectonophysics, v. 273, n. 1–2, p. 105–127, http://dx.doi.org/10.1016/S0040-1951(96)00290-9

Cobiella-Reguera, J. L., 1988, El vulcanismo paleogénico cubano, apuntes para un nuevo enfoque: Revista Tecnológica, v. 18, n. 4, p. 25–32.

——— 2000, Jurassic and Cretaceous geological history of Cuba: International Geology Review, v. 42, n. 7, p. 594–616, http://dx.doi.org/10.1080/00206810009465102

——— 2005, Emplacement of Cuban ophiolites: Geológica Acta, v. 3, n. 3, p. 273–294.

Cruz-Gámez, E. M., Maresch, W. V., Cáceres-Govea, D., and Balcazar, N., 2007, Significado de las paragènesis de anfíboles en metagabros relacionados con secuencias de margen continental en el NW de Cuba: Revista Mexicana de Ciencias Geológicas, v. 24, n. 3, p. 318–327.

Cruz-Orosa, I., Sàbat, F., Ramos, E., Rivero, L., and Vázquez-Taset, Y. M., 2012a, Structural evolution of the La Trocha fault zone: Oblique collision and strike-slip basins in the Cuban Orogen: Tectonics, v. 31, n. 5, article number TC5001, http://dx.doi.org/10.1029/2011TC003045

Cruz-Orosa, I., Sàbat, F., Ramos, E., and Vázquez-Taset, Y. M., 2012b, Synorogenic basins of central Cuba and collision between the Caribbean and North American plates: International Geology Review, v. 54, n. 8, p. 876–906, http://dx.doi.org/10.1080/00206814.2011.585031

Despaigne-Díaz, A. I., ms, 2009, Estructura y metamorfismo del área La Sierrita, macizo Escambray, Central Cuba: Cuba, Pinar del Río, Universidad de Pinar del Río, Ph. D. thesis, 187 p.

Despaigne-Díaz, A. I., and Cáceres Govea., D., 2009a, Análisis estructural de la zona de Yaguanabo, macizo Escambray, Cuba Central, aplicando criterios macro y microtectónicos: Revista Geología y Minería, v. 25, n. 1, p. 1–33.

——— 2009b, Las maclas de calcita en los metacarbonatos. Significado tectónico y su empleo para la determinación de temperaturas de deformación: Revista Geología y Minería, v. 25, n. 2, p. 1–31.

Draper, G., 2001, The metamorphic terranes of Cuba as metamorphic core complexes exhumed by low-angle normal faulting?: Reunión del proyecto No. 433 PICG/UNESCO "Tectonica de placas del Caribe".

Draper, G., Jackson, T. A., and Donovan, S. K., 1994, Geologic provinces of the Caribbean Region, *in* Donovan, S. K., and Jackson, T. A., editors, Caribbean Geology: An Introduction: Kingston, Jamaica, University of West Indies Publishers' Association/University of the West Indies Press, p. 3–12.

Dryar, M. D., Colucci, M. T., and Guidotti, C. V., 1991, Forgotten major elements: Hydrogen and oxygen variation in biotite from metapelites: Geology, v. 19, n. 10, p. 1029–1032, http://dx.doi.org/10.1130/0091-7613(1991)019<1029:FMEHAO>2.3.CO;2

Dublan, L., Álvarez-Sánchez, H., Mlcoch, B., Mañour, J., LLedíaz, P., Molak, B., Vázquez, C., Snopkova, P., De los Santos, E., Soucek, J., Pérez, M., Mihailova, A., Bernal, I., Zoubek, J., Ordoñez, M., Soucek, J., Morousek, J., Svetska, J., Marshall, W., Pérez-Conde, R., González, E., and Rodríguez, R., 1986, Informe final del levantamiento geológico y evaluación de minerales utiles, a escala 1:50 000, del poligono CAME I, zona Centro: La Habana, Cuba, Fondo Geológico Nacional, Oficina Nacional de Recursos Minerales, Ministerio de Industria Bàsica, 1402 p., 250 maps (unpublished report).

Escuder-Viruete, J., and Pérez-Estaún, A., 2006, Subduction-related *P-T* path for eclogites and garnet glaucophanites from the Samaná Peninsula basement complex, northern Hispaniola: International Journal of Earth Sciences v. 95, n. 6, p. 995–1017, http://dx.doi.org/10.1007/s00531-006-0079-5

Escuder-Viruete, J., Pérez-Estaún, A., Gabites, J., and Suárez-Rodriguez, A., 2011a, Structural development of a high-pressure collisional accretionary wedge: The Samaná complex, Northern Hispaniola: Journal of Structural Geology, v. 33, n. 5, p. 928–950, http://dx.doi.org/10.1016/j.jsg.2011.02.006

Escuder-Viruete, J., Pérez-Estaún, A., Booth-Rea, G., and Valverde-Vaquero, P., 2011b, Tectonometamorphic evolution of the Samaná complex, northern Hispaniola: Implications for the burial and exhumation of high-pressure rocks in a collisional accretionary wedge: Lithos, v. 125, n. 1–2, p. 190–210, http://dx.doi.org/10.1016/j.lithos.2011.02.006

Escuder-Viruete, J., Valverde-Vaquero, P., Rojas-Agramonte, Y., Gabites, J., Castillo-Carrión, M., and Pérez-

Estaún, A., 2013, Timing of deformational events in the Río San Juan complex: Implications for the tectonic controls on the exhumation of high-P rocks in the northern Caribbean subduction-accretionary prism: Lithos, v. 177, p. 416–435, http://dx.doi.org/10.1016/j.lithos.2013.07.006
Fonseca, E., Gonzalez, R., Delgado, R., and Savieleva, G., 1989, Presencia de efusivos ofioliticos y boninitas en las provincias de La Habana y Matanzas: Boletin técnico de Geologia, v. 1, p. 1–9.
García-Casco, A., Torres-Roldán, R. L., Millán, G., Monié, P., and Haissen, F., 2001, High-grade metamorphism and hydrous melting of metapelites in the Pinos terrane (W Cuba): Evidence for crustal thickening and extension in the northern Caribbean Collisional belt: Journal of Metamorphic Geology, v. 19, n. 6, p. 699–715, http://dx.doi.org/10.1046/j.0263-4929.2001.00343.x
García-Casco, A., Torres-Roldán, R. L., Millán, G., Monié, P., and Schneider, J., 2004, Oscillatory zoning in eclogite garnet and amphibolite, Northern Serpentinite Mélange, Cuba: A record of tectonic instability during subduction?: Journal of Metamorphic Geology, v. 20, n. 6, p. 581–598, http://dx.doi.org/10.1046/j.1525-1314.2002.00390.x
García-Casco, A., Torres-Roldán, R. L., Iturralde-Vinent, M. A., Millán Trujillo, G., Núñez Cambra, K., Lázaro, C., and Rodríguez Vega, A., 2006, High pressure metamorphism of ophiolites in Cuba: Geologica Acta, v. 4, n. 1–2, p. 63–88.
García-Casco, A., Iturralde-Vinent, M. A., and Pindell, J., 2008a, Latest Cretaceous collision/accretion between the Caribbean plate and Caribeana: Origin of metamorphic complexes in the Greater Antilles: International Geology Review, v. 50, n. 9, p. 781–809, http://dx.doi.org/10.2747/0020-6814.50.9.781
García-Casco, A., Lázaro, C., Torres-Roldán, R. L., Núñez, K., Rojas-Agramonte, Y., Kröner, A., Neubauer, F., Millán, G., and Blanco-Quintero, I., 2008b, Partial melting and counterclokwise *P-T* path of subducted oceanic crust (Sierra del Convento Mélange, Cuba): Journal of Petrology, v. 49, n. 1, p. 129–161, http://dx.doi.org/10.1093/petrology/egm074
Grafe, F., Stanek, K. P., Baumann, A., Maresch, W. V., Hames, W. E., Grevel, C., and Millán, G., 2001, Rb-Sr and $^{40}Ar/^{39}Ar$ mineral ages of granitoid intusives in the Mabujina unit, Central Cuba: Thermal exhumation history of the Escambray massif: Journal of Geology, v. 109, n. 5, p. 615–631, http://dx.doi.org/10.1086/321966
Grevel, C., ms, 2000, Druck und Temperaturentwicklung der metamorphen Deckneinheiten des Escambray másives, Kuba (Pressure and temperature history of the metamorphic nappes of the Escambray mássif, (Cuba): Bochum, Germany, Ruhr-Universitat Bochum, Ph. D. thesis, 170 p.
Guidotti, C. V., 1978, Compositional variation of muscovite in medium to high grade metapelites of Northwestern Maine: American Mineralogist, v. 63, n. 9–10, p. 878–884.
——— 1984, Micas in metamorphic rocks, *in* Bailey, S. W., editor, Micas: Reviews in Mineralogy, v. 13, p. 357–468.
Guidotti, C. V., and Dryar, M. D., 1991, Ferric iron in metamorphic biotite and its petrologic y crystallochemical implications: American Mineralogist, v. 76, n. 1–2, p. 161–175.
Guidotti, C. V., Cheney, J. T., and Guggennheim, S., 1977, Distribution of titanium between coexisting muscovite and biotite in pelitic schists from northwestern Maine: American Mineralogist, v. 62, n. 5–6, p. 438–448.
Hatten, C. W., Somin, M. L., Millán, G., Renne, P., Kistler, R. W., and Mattinson, J. M., 1988, Tectonoestratigraphic units of Central Cuba: Barbados, Transactions of the 11th Caribbean Geological Conference Barbados, v. 35, p. 1–13.
Hatten, C. W., Mattinson, J. M., Renne, P. R., Somin, M. L., Millán, G., Araqueliants, M. M., Kolesnikov, E. M., and Sumin, L. V., 1989, Rocas metamórficas dealta presión: nuevos datos acerca de sus edades: La Habana, Cuba, Primer Congreso Cubano de Geología, Memorias, p. 118–119.
Henry, D. J., Guidotti, C. V., and Thomson, J. A., 2005, The Ti-saturation surface for low-to-medium pressure metapelitic biotites: Implications for geothermometry and Ti-substitution mechanisms: American Mineralogist, v. 90, n. 2–3, p. 316–328, http://dx.doi.org/10.2138/am.2005.1498
Iturralde-Vinent, M. A., 1988, Consideraciones generales sobre el magmatismo de margen continental de Cuba: Revista Tecnológica, v. 18, p. 17–24.
——— 1994, Cuban geology: A new plate tectonic synthesis: Journal of Petroleum Geology, v. 17, n. 1, p. 39–70, http://dx.doi.org/10.1111/j.1747-5457.1994.tb00113.x
——— 1996a, Introduction to Cuban Geology and Geophysics, *in* Iturralde-Vinent, M. A., editor, Ofiolitas y Arcos Volcánicos de Cuba: IGCP Project 364, Special Contribution, v. 1, p. 3–35.
——— 1996b, El arco de islas volcánicas del Cretácico *in* Iturralde-Vinent, M. A., editor, Ofiolitas y Arcos volcánicos de cuba: Miami, USA, IGCP Project 364, Special Contribution, v. 1, p. 179–189.
——— 1998, Sinopsis de la constitución Geológica de Cuba: Acta Geológica Hispánica, v. 33, p. 9–59.
——— 1998, Naturaleza geológica de Cuba, La Habana, Cuba: Editorial Científico-Tectónica, 246 p.
Iturralde-Vinent, M. A., and Lidiak, E. G., 2006, Caribbean tectonic, magmatic, metamorphic and stratigraphic events. Implications for plate tectonics: Geologica Acta, v. 4, p. 1–5.
Iturralde-Vinent, M. A., Millán, G., Korkas, L., Nagy, E., and Pajón, J., 1996, Geological interpretation of the Cuba K-Ar data base *in* Iturralde-Vinent, M. A., editor, Ofiolitas y Arcos Volcánicos de Cuba: IGCP Project 364, Special Contribution, v. 1, p. 48–69.
Iturralde-Vinent, M. A., Diaz Otero, C., García-Casco, A., and Van Hinsbergen, D. J. J., 2008, Paleogene Foredeep Basin Deposits of North-Central Cuba: A Record of Arc-Continent Collision between the Caribbean and North American Plates: International Geology Review, v. 50, n. 10, p. 863–884, http://dx.doi.org/10.2747/0020-6814.50.10.863
Joyce, J., 1991, Blueschist metamorphism and deformation on the Samaná Peninsula; A record of subduction and collision in the Greater Antilles, *in* Mann, P., Draper, G., and Lewis, J. F., editors, Geologic and Tectonic Development of the North America-Caribbean Plate Boundary in Hispaniola: Geological Society of America Special Paper, v. 262, p. 47–76, http://dx.doi.org/10.1130/SPE262-p47
Kantchev, I., 1978, Informe geológico de la provincia Las Villas-Resultados de las investigaciones geológicas a

escala 1: 250 000 durante el periodo 1969–1975: Oficina Nacional de Recursos Minerales, Ministerio de Industria Básica, La Habana, Cuba, (unpublished report), 1480 p.

Kerr, A. C., Iturralde-Vinent, M. A., Saunders, A. D., Babbs, T. L., and Tarney, J., 1999, A new plate tectonic model of the Caribbean: Implications from a geochemical reconnaissance of Cuban Mesozoic Volcanic rocks: Geological Society of America Bulletin, v. 111, n. 11, p. 1581–1599, http://dx.doi.org/10.1130/0016-7606(1999)111<1581:ANPTMO>2.3.CO;2

Kimura, G., Maruyama, S., Isozaki, Y., and Terabayashi, M., 1996, Well preserved underplating structure of the jadeitized Franciscan complex, Pacheco Pass, California: Geology, v. 24, n. 1, p. 75–78, http://dx.doi.org/10.1130/0091-7613(1996)024<0075:WPUSOT>2.3.CO;2

Kirschner, D. L., Cosca, M. A., Mason, H., and Hunziker, J. C., 1996, Staircase $^{40}Ar/^{39}Ar$ spectra of fine-grained white mica: Timing and duration of deformation and empirical constraints on argon diffusion: Geology, v. 24, n. 8, p. 747–750, http://dx.doi.org/10.1130/0091-7613(1996)024<0747:SAASOF>2.3.CO;2

Koppers, A. A. P., 2002, ArArCALC-software for $^{40}Ar/^{39}Ar$ age calculations: Computers & Geosciences, v. 28, n. 5, p. 605–619, http://dx.doi.org/10.1016/S0098-3004(01)00095-4

Krebs, M., Maresh, W. V., Schertl, H. P., Münker, C., Baumann, A., Draper, G., Idleman, B., and Trapp, E., 2008, The dynamics of intra-oceanic subduction zones: A direct comparison between fossil petrological evidence (Rio San Juan Complex, Dominican Republic) and numerical simulation: Lithos, v. 103, p. 106-137, http://dx.doi.org/10.1016/j.lithos.2007.09.003

Lázaro, C., and García-Casco, A., 2008, Geochemical and Sr-Nd isotope signatures of pristine slab melts and their residues (Sierra del Convento mélange, eastern Cuba): Chemical Geology, v. 255, n. 1–2, p. 120–13, http://dx.doi.org/10.1016/j.chemgeo.2008.06.017

Lázaro, C., García-Casco, A., Neubaurer, F., Rojas-Agramonte, Y., Kröner, A., and Iturralde- Vinent, M., 2009, Fifty-five-million-year history of oceanic subduction and exhumation at the northern edge of the Caribbean plate (Sierra del Convento mélange, Cuba): Journal of Metamorphic Geology, v. 27, n. 1, p. 19–40, http://dx.doi.org/10.1111/j.1525-1314.2008.00800.x

Leake, B. E., Wolley, A. R., Arps, C. E. S., Birch, W. D., Gilbert, M. C., Grice, J. D., Hawthorne, F. C., Kato, A., Kisch, H. J., Krivovichev, V. G., Linthout, K., Laird, J., Mandarino, J. A., Maresch, W. V., Nickel, E. H., Rock, N. M. S., Schumacher, J. C., Smith, D. C., Stephenson, N. C. N., Ungaretti, L., Whittaker, E. J. W., and Youzhi, G., 1997, Nomenclature of amphiboles: Report of the Subcommittee on Amphiboles of the International Mineralogical Association, Commission on New Minerals and Mineral Names: American Mineralogist, v. 82, p. 1019–1037, http://dx.doi.org/10.1180/minmag.1997.061.405.13

Lee, J. Y., Marti, K., Severinghaus, J. P., Kawamura, K., Yoo, H. S., Lee, J. B., and Kim, J. S, 2006, A redetermination of the isotopic abundances of atmospheric Ar: Geochimica et Cosmochimica. Acta, v. 70, n. 17, p. 4507–4512, http://dx.doi.org/10.1016/j.gca.2006.06.1563

Liou, J. G., Tsujimori, T., Zhang, R. Y., Katayama, I., and Maruyama, S., 2004, Global UHP Metamorphism and Continental Subduction/Collision: The Himalayan Model: International Geology Review, v. 46, n. 1, p. 1–27, http://dx.doi.org/10.2747/0020-6814.46.1.1

Mann, P., 1999, Caribbean sedimentary basins: Classification and Tectonic Setting from Jurassic to Present, *in* Mann, P., editor, Caribbean Basins: Sedimentary Basins of the World, v. 4, p. 3–31, http://dx.doi.org/10.1016/S1874-5997(99)80035-5

Maresch, W. V., Stanek, K. P., Grafe, F., Idleman, B., Baumann, A., Krebs, M., Schertl, H. P., and Draper, G., 2003, Age systematics of high-pressure metamorphism in the Caribbean: confronting existing models with new data: La Habana, Cuba, 5th Cuban geological Congress, GEOMIN 2003, Memorias, p. 296–298, SBN 959-7117-11-8, 39.

Massone, H. J., and Shreyer, W., 1987, Phengite geobarometry based on the limiting assemblage with K-feldspar, phlogopite and quartz: Contributions to Mineralogy and Petrology, v. 96, n. 2, p. 212–224, http://dx.doi.org/10.1007/BF00375235

Massone, H. J., and Szpurka, Z., 1997, Thermodynamic properties of white micas on the basis of high-pressure experiments in the systems K_2O-MgO-Al_2O3-SiO_2 and K_2O-FeO-Al_2O_3-SiO_2-H_2O: Lithos, v. 41, n. 1–3, p. 229–250, http://dx.doi.org/10.1016/S0024-4937(97)82014-2

Meschede, M., and Frisch, W., 1998, A plate-tectonic model for the Mesozoic and Early Cenozoic history of the Caribbean plate: Tectonophysics, v. 296, n. 3–4, p. 269–291, http://dx.doi.org/10.1016/S0040-1951(98)00157-7

Meyerhoff, A. A., and Hatten, C. W., 1968, Diapiric structures in central Cuba, *in* Braunstein, I., and O'Brien, G. D., editors, Diapirism and Diapirs: American Association of Petroleum Geologists Memoir, v. 8, p. 315–357.

Millán, G., 1981, Geología del macizo metamórfico de la Isla de la Juventud: Ciencias de la Tierra y del Espacio, v. 3, p. 3–22.

——— Metamorfitas de la asociación ofiolítica de Cuba *in* Iturralde-Vinent, M. A., editor, Ofiolitas y arcos volcánicos de Cuba: Miami, Florida, USA, IGCP project 364, Special contribution, v. 1, p. 131–146.

——— 1996b, Geología del complejo de Mabujina *in* Iturralde-Vinent, M. A., editor, Ofiolitas y Arcos Volcánicos de Cuba: Miami, Florida, USA, IGCP Project 364 Special Contribution, v. 1, p. 147–153.

——— 1997a, Posición estratigráfica de las metamorfitas cubanas *in* Furrazola Bermudez, G. F., and Nuñez Cambra, K. E., editors, Estudios sobre Geología de Cuba: La Habana, Cuba, Centro Nacional de Información geológica, p. 251–258.

——— 1997b, Geologia del macizo metamórfico del Escambray *in* Furrazola Bermudez, G. F., and Nuñez Cambra, K. E., editors, Estudios sobre Geología de Cuba: La Habana, Cuba, Centro Nacional de Información geológica, p. 271–288.

Millán, G., and Álvarez-Sánchez, H., 1992, Geología del sector de La Sierrita. Cúpula de Trinidad. Macizo Metamórfico Escambray: Unpublished report of the Instituto de Geología y Paleontología, La Habana, y Empresa de Geología de Santa Clara, Cuba, 40 p.

Millán, G., and Myczynski, R., 1978, Fauna Jurásica y consideraciones sobre la edad de las secuencias metamórficas del Escambray: Academia de Ciencias de Cuba, Informe Científico Técnico, v. 80, p. 1–14.
Millán, G., and Somin, M. L., 1985, Contribución al conocimiento geológico de las metamorfitas del Escambray y Purial: Reportes de la Investigación de la Academia de Ciencias de Cuba, v. 2, p. 1–74.
McDougall, I., and Harrison, T. M., 1999, Geochronology and Thermochronology by the $^{40}Ar/^{39}Ar$ Method: New York, Oxford University Press, 269 p.
Otsuki, M., and Bano, S., 1990, Prograde and retrograde metamorphism of hematite bearing basic schists in the Sanbagawa belt in central Shikoku: Journal of Metamorphic Geology, v. 8, n. 4, p. 425–439, http://dx.doi.org/10.1111/j.1525-1314.1990.tb00629.x
Passchier, C. W., and Trouw, R. A., 1998, Microtectonics: Berlin, Springer Verlag. Second Edition, 289 p.
Peacock, S. M., and Wang, K., 1999, Seismic Consequences of Warm Versus Cool Subduction metamorphism: Examples from Southwest and Northeast Japan: Science, v. 286, n. 5441, p. 937–939, http://dx.doi.org/10.1126/science.286.5441.937
Peacock, S. M., Rushmer, T., and Thompson, A. B., 1994, Partial melting of subducting oceanic crust: Earth and Planetary Science Letters, v. 121, n. 1–2, p. 227–244, http://dx.doi.org/10.1016/0012-821X(94)90042-6
Perfit, M. R., Heezen, B. C., Rawson, M., and Donnelly, T. W., 1980, Chemistry, origin and tectonic significance of metamorphic rocks from the Puerto Rico Trench: Marine Geology, v. 34, n. 1–2, p. 125–156, http://dx.doi.org/10.1016/0025-3227(80)90069-9
Pindell, J. L., and Kennan, L., 2009, Tectonic evolution of the Gulf of Mexico, Caribbean and northern South America in the mantle reference frame: an update *in* James, K. H., Lorente, M. A., and Pindell, J. L., editors, The Origin and Evolution of the Caribbean Plate: Geological Society of London, Special Publications, v. 328, p. 1–55, http://dx.doi.org/10.1144/SP328.1
Pindell, J. L., Kennan, L., Maresch, W. V., Stanek, K. P., Draper, G., and Higgs, R., 2005, Plate-kinematics and crustal dynamics of circum-Caribbean arc-continent interactions: Tectonic controls on basin development in Proto-Caribbean margins *in* Avé Lallemant, H. G., and Sisson, V. B., editors, Caribbean-South American plate interactions, Venezuela: Geological Society of America Special Papers 394, p. 7–52, http://dx.doi.org/ 10.1130/0-8137-2394-9.7
Pindell, J. L, Kennan, L., Stanek, K. P., Maresch, W. V., and Draper, G., 2006, Foundations of Gulf of Mexico and Caribbean evolution: eight controversies resolved: Geologica Acta, v. 4, n. 1–2, p. 303–341.
Platt, J. P., 1993, Exhumation of high-pressure rocks: a review of concepts and processes: Terra Nova, v. 5, n. 2, p. 119–133, http://dx.doi.org/10.1111/j.1365-3121.1993.tb00237.x
Pszczolkowski, A., 1999, The exposed passive margin of North America in western Cuba, *in* Mann, P., editor, Caribbean Basins: Sedimentary Basins of the World, v. 4, p. 93–121, http://dx.doi.org/10.1016/S1874-5997(99)80038-0
Purdy, J. W., and Jaeger, E., 1976, K-Ar ages on rock forming minerals from the central Alps: Padua, Italy, Memorial Institute of Geology and Mineralogy, University of Padova, v. 30, p. 1–31.
Pushcharovsky, Yu. M., Mossakovsky, A. A., and Nekrasov, G. E., 1989, Nota explicativa al Mapa Geológico de Cuba a escala 1:250 000: Moscow, Russia, Instituto de Geología, Academia de Ciencias (in Russian).
Pyle, T. E., Meyerhoff, A. A., Fahlquist, D. A., Antoine, J. W., McCrevey, J. A., and Jones, P. C., 1973, Metamorphic rocks from northwestern Caribbean Sea: Earth and Planetary Science Letters, v. 18, n. 2, p. 339–344, http://dx.doi.org/10.1016/0012-821X(73)90074-5
Renne, P. R., Mundil, R., Balco, G., Min, K., and Ludwig, K. R., 2010, Joint determination of ^{40}K decay constants and $^{40}Ar/^{40}K$ for the Fish Canyon sanidine standard, and improved accuracy for $^{40}Ar/^{39}Ar$ geochronology: Geochimica et Cosmochimica Acta, v. 74, n. 18, p. 5349–5367, http://dx.doi.org/10.1016/j.gca.2010.06.017
Renne, P. R., Balco, G., Ludwig, K. R., Mundil, R., and Min, K., 2011, Response to the comment by W.H. Schwarz et al. on "Joint determination of ^{40}K decay constants and $^{40}Ar^*/^{40}K$ for the Fish Canyon sanidine standard, and improved accuracy for $^{40}Ar/^{39}Ar$ geochronology" by P.R. Renne et al. (2010): Geochimica et Cosmochimica Acta, v. 75, n. 17, p. 5097–5100, http://dx.doi.org/10.1016/j.gca.2011.06.021
Rojas-Agramonte, Y., Neubauer, F., Bojar, A. V., Hejl, E., Handler, R., and García-Delgado, D. E., 2006, Geology, age and tectonic evolution of the Sierra Maestra Mountains, southeastern Cuba: Geologica Acta, v. 4, n. 1–2, p. 123–150.
Rojas-Agramonte, Y., Neubauer, F., Garcia-Delgado, D. E., Handler, R., Fried, G., and Delgado-Damas, R., 2008, Tectonic evolution of the Sierra Maestra Mountains, SE Cuba, during Tertiary times: From arc-continent collision to transform motion: Journal of South American Earth Sciences, v. 26, n. 2, p. 125–151, http://dx.doi.org/10.1016/j.jsames.2008.05.005
Rojas-Agramonte Y., Kröner, A., García-Casco, A., Kempt, T., Hegner, E., Pérez, M., Barth, M., Liu, D., and Fonseca-Montero, A., 2010, Zircon ages, Sr-Nd-Hf isotopic compositions, and geochemistry of granitoids associated with the northern ophiolite mélange of central Cuba: Tectonic implication for late Cretaceous magmatism in the northwestern Caribbean: American Journal of Science, v. 310, n. 10, p. 1453–1479, http://dx.doi.org/10.2475/10.2010.09
Rojas-Agramonte Y., Kröner, A., García-Casco, A., Iturralde-Vinent, M. A., Somin, M., Mattinson, J. M., Millán-Trujillo, G., Sukar, K., Pérez-Rodriguez, M., Carrasquilla, S., Wingate, M. T. D., and Liu, D. Y., 2011, Timing and Evolution of Cretaceous Island Arc Magmatism in Central Cuba: Implications for the History of Arc Systems in the Northwestern Caribbean: The Journal of Geology, v. 119, n. 6, p. 619–640, http://dx.doi.org/10.1086/662033
Saura, E., Vergés, J., Brown, D., Lukito, P., Soriano, S., Torrescusa, S., García, R., Sánchez, J. R., Sosa, C., and Tenreyro, R., 2008, Structural and tectonic evolution of western Cuba fold and thrust belt: Tectonics, v. 27, n. 4, TC400, http://dx.doi.org/10.1029/2007TC002237
Sigurdsson, H., Kelley, S., Leckie, R. M., Brallower, T., and King, J., 2000, History of Circum- Caribbean

explosive volcanism: $^{40}Ar/^{39}$ Ar dating of tephra layers, *in* Leckie, R. M., Sigurdsson, H., Acton, G. D., and Draper, G., editors, 2000 Proceedings of the Ocean Drilling Program: Scientific Results, v. 165, p. 299–314, http://dx.doi.org/10.2973/odp.proc.sr.165.021.2000

Simpson, G. D. H., Thompson, A. B., and Connolly, J. A. D., 2000, Phase relations, singularities and thermobarometry of metamorphic assemblages containing phengite, chlorite, biotite, K-feldspar, quartz and H_2O: Contributions to Mineralogy and Petrology, v. 139, n. 5, p. 555–569, http://dx.doi.org/10.1007/s004100000154

Somin, M., and Millán, G., 1972, The metamorphic complexes of Pinos, Escambray and Oriente in Cuba and its ages (in Russian): Izvestia Akad Nauk SSSR, Geology, v. 5, p. 48–57.

——— 1981, Geology of the Metamorphic Complex of Cuba: Nauka, Moscow, 219 p. (in Russian).

Somin, M. L., Arakelyants, M. M., and Kolesnikov, E. M., 1992, Age and tectonic significance of high-pressure metamorphic rocks in Cuba: International Geology Review, v. 34, n. 2, p. 105–118, http://dx.doi.org/10.1080/00206819209465587

Schneider, J., Bosch, D., Monie, P., Guillot, S., García-Casco, A., Lardeaux, J. M., Torres-Roldán, R. L., and Millán Trujillo, G., 2004, Origin and evolution of the Escambray massif (central Cuba): an example of HP/LT rocks exhumed during intraoceanic subduction: Journal of Metamorphic Geology, v. 22, n. 3, p. 227–247, http://dx.doi.org/10.1111/j.1525-1314.2004.00510.x

Stanek, K. P., and Maresch, W. V., 2007, Timing of the HP metamorphism of the Escambray massif, Central Cuba *in* Martens, U., and García-Casco, A., editors, High-pressure belts of central Guatemala: The Motagua suture and the Chuacús Complex: IGCP 546 Special Contribution, v.1 [http://www.ugr.es/~agcasco/igcp546/].

Stanek, K. P., Maresch, W. V., Grafe, F., Grevel, Ch., and Baumann, A., 2006, Structure, tectonics and metamorphic development of the Sancti Spiritus dome (eastern Escambray massif, Central Cuba): Geologica Acta, v. 4, n. 1–2, p. 151–170.

Stanik, E., Ching, R., Mañour, J., and Vázquez, C., 1981, Informe del levantamiento geológico Escambray I: Empresa Geominera del Centro (unpublished report), 512 p.

Van Hinsbergen, D. J. J., Iturralde-Vinent, M. A., Van Geffen, P. W. G., García-Casco, A., and Van Benthem, S., 2009, Structure of the accretionary prims and the evolution of the Paleogene northern Caribbean subduction zone in the region of Camaguey, Cuba: Journal of Structural Geology, v. 31, n. 10, p. 1130–1144, http://dx.doi.org/10.1016/j.jsg.2009.06.007

Wijbrans, J., and McDougall, I., 1986, $^{40}Ar/^{39}Ar$ dating of white micas from an Alpine high-pressure metamorphic belt on Naxos (Greece): The resetting of the argon isotopic system: Contributions to Mineralogy and Petrology, v. 93, n. 2, p. 187–194, http://dx.doi.org/10.1007/BF00371320

Whitney, D. L., and Evans, B. W., 2010. Abbreviations for names of rock-forming minerals: American Mineralogist, v. 95, n. 1, p. 185–187, http://dx.doi.org/10.2138/am.2010.3371

Zwart, H. J., 1960, The chronological succession of folding and metamorphism in the Central Pyrenees: Geologische Rundschau, v. 50, n. 1, p. 203–218, http://dx.doi.org/10.1007/BF01786838

——— 1962, On the determination of polymetamorphic mineral associations, and its application to the Bosost area (Central Pyrenees): Geologische Rundschau, v. 52, n. 1, p. 38–65, http://dx.doi.org/10.1007/BF01840064